NTIS # PB2022-

SSC-477
EXPLORING THE SUITABILITY OF COMMERCIAL OFF-THE-SHELF STRUCTURAL HEALTH MONITORING HARDWARE AND SOFTWARE FOR NAVAL USE

SHIP STRUCTURE COMMITTEE

2022

Member Agencies:

American Bureau of Shipping
Defence Research & Development Canada
Maritime Administration
Military Sealift Command
Naval Sea Systems Command
Office of Naval Research
Society of Naval Architects & Marine Engineers
Transport Canada
United States Coast Guard

Ship
Structure
Committee

Address Correspondence to:

Commandant (CG-ENG-2/SSC)
ATTN: Executive Director, SSC
US Coast Guard
2703 Martin Luther King Jr. Ave SE
Washington, DC 20593-7509
Website: http://www.shipstructure.org

SSC – 477
SR – 1480

10 August 2022

EXPLORING THE SUITABILITY OF COMMERCIAL OFF-THE-SHELF STRUCTURAL HEALTH MONITORING HARDWARE AND SOFTWARE FOR NAVAL USE

With the ongoing development of structural health monitoring sensors, data acquisition hardware, and data processing techniques; the value of continuous structural monitoring on ships is becoming more apparent. Structural health monitoring is especially valuable for tracking fatigue life and can be of great assistance for extension of ship service life or fleet management decisions.

This study investigates new commercial off-the-shelf structural health monitoring hardware developed under small business funding from the U.S. Navy, U.S. Air Force, and National Aeronautics and Space Administration to determine how it can be used aboard Naval vessels. The study finds considerable value added when structural health monitoring hardware is used at critical or difficult to inspect areas in conjunction with regular visual inspection and non-destructive examination. Using a combination of these methods results in a more comprehensive understanding of a vessel's overall structural condition.

We thank the authors and Project Technical Committee for their dedication and research toward completing the objectives and tasks detailed throughout this paper and continuing the Ship Structure Committee's mission to enhance the safety of life at sea.

W. R. ARGUIN
Rear Admiral, U.S. Coast Guard
Co-Chair, Ship Structure Committee

J. M. LLOYD
Rear Admiral, U.S. Navy
Co-Chair, Ship Structure Committee

SHIP STRUCTURE COMMITTEE

RADM Wayne Arguin
U. S. Coast Guard Assistant Commandant
for Prevention Policy (CG-5P)
Co-Chair, Ship Structure Committee

RDML Jason Lloyd
Chief Engineer and Deputy Commander
For Naval Systems Engineering (SEA05)
Co-Chair, Ship Structure Committee

Mr. Jeffrey Lantz
Director, Commercial Regulations and Standards (CG-5PS)
U.S. Coast Guard

Mr. Gareth Burton
Vice President, Technology
American Bureau of Shipping

Mr. H. Paul Cojeen
Society of Naval Architects and Marine Engineers

Dr. John MacKay
Head, Warship Performance, DGSTCO
Defence Research & Development Canada - Atlantic

Mr. Kevin Kohlmann
Director, Office of Safety
Maritime Administration

Mr. Luc Tremblay
Executive Director, Domestic Vessel Regulatory Oversight
and Boating Safety, Transport Canada

Mr. Albert Curry
Deputy Assistant Commandant for Engineering and
Logistics (CG-4D)
U.S. Coast Guard

Mr. Eric Duncan
Group Director, Ship Integrity and Performance Engineering
(SEA 05P)
Naval Sea Systems Command

Mr. Neil Lichtenstein
Deputy Director N7x, Engineering Directorate
Military Sealift Command

Dr. Thomas Fu
Director, Ship Systems and Engineering Research Division
Office of Naval Research

SHIP STRUCTURE EXECUTIVE GROUP & SUB-COMMITTEE

UNITED STATES COAST GUARD (CVE)
CAPT Daniel Cost
Mr. Jaideep Sirkar
Mr. Charles Rawson

AMERICAN BUREAU OF SHIPPING
Dr. Qing Yu
Dr. Gu Hai
Mr. Daniel LaMere
Ms. Christina Wang
Mr. Rich Delpizzo

SOCIETY OF NAVAL ARCHITECTS AND MARINE ENGINEERS
Mr. Frederick Ashcroft
Dr. Roger Basu
Dr. Robert Sielski
Dr. Paul Miller

DEFENCE RESEARCH & DEVELOPMENT CANADA ATLANTIC
Dr. Malcolm Smith
Mr. Cameron Munro
Mr. Neil Pegg

MARITIME ADMINISTRATION
Mr. Todd Ripley

TRANSPORT CANADA
Ms. Veronique Bérubé
Mr. Bashir Ahmed Golam
Ms. Tayyebe Seif

UNITED STATES COAST GUARD (FLEET)
CAPT Christopher Wolfe
Mr. Martin Hecker
Mr. Timothy McAllister
Mr. Debu Ghosh

NAVSEA/ NSWCCD
Mr. David Qualley
Mr. Dean Schleicher
Dr. Pradeep Sensharma
Mr. Daniel Bruchman

MILITARY SEALIFT COMMAND
Ms. Jeannette Viernes

OFFICE OF NAVAL RESEARCH
Dr. Paul Hess

PROJECT TECHNICAL COMMITTEE

The Ship Structure Committee greatly appreciates the contributions of the individuals that volunteered their time to participate on the Project Technical Committee, listed below, and thanks them heartily. They were the subject matter expert representatives of the Ship Structure Committee to the contractor, performing technical oversight during contracting, advising the contractor in cognizant matters pertaining to the contract of which the agencies were aware, and performing technical peer review of the work in progress and upon completion.

Chair:

David Qualley, Naval Sea Systems Command

Members:

Jason Cordell, Naval Sea Systems Command
Damian McGuckin, Pacific ESI
Dr. Haitao Liu, American Bureau of Shipping
Keith Hennessy, Irving Shipbuilding
Dr. Paul Hess, Office of Naval Research
Ian Thompson, Defense Research and Development Canada

Ship Structure Committee Executive Director:

LCDR Bryan J. Andrews, U.S. Coast Guard

Technical Report Documentation Page

1. Report No.	2. Government Accession No.	3. Recipient's Catalog No.
4. Title and Subtitle Exploring the Suitability of Commercial off-the-Shelf Structural Health Monitoring Hardware and Software for Naval Use		5. Report Date February 2021 6. Performing Organization Code
7. Author(s) Grisso, B. L.		8. Performing Organization Report No. SR-1480
9. Performing Organization Name and Address Naval Surface Warfare Center, Carderock Division 9500 MacArthur Blvd West Bethesda, MD 20817		10. Work Unit No. (TRAIS) 11. Contract or Grant No. N0002418WX09495
12. Sponsoring Agency Name and Address COMMANDANT (CG-5212/SSC) ATTN (ADMIN ASST/SHIP STRUCTURE COMMITTEE) U S COAST GUARD 2100 2ND ST SW STOP 7126 WASHINGTON DC 20593-7126		13. Type of Report and Period Covered Final Report 6/18-9/19 14. Sponsoring Agency Code G-M
15. Supplementary Notes Sponsored by the Ship Structure Committee. Jointly funded by its member agencies.		

16. Abstract

The U.S. Navy, Air Force, National Aeronautics and Space Administration and other organizations have all contributed to the development of structural health monitoring sensors, data acquisition hardware, and techniques to process and interpret the resulting data for use on everything from civil infrastructure to space vehicles. One promising suite of sensors and data acquisition hardware, developed under multiple contracts with the U.S. Department of Defense and National Aeronautics and Space Administration, was recently licensed for commercial development and production. The study detailed in this report investigates whether the new commercial off-the-shelf structural health monitoring hardware is suitable for use on Navy or commercial surface vessels and, if not, what improvements or modifications the Navy should investigate to develop a health monitoring system capable of detecting defects within in-service ship structures.

17. Key Words	18. Distribution Statement
Structural Health Monitoring, Continuous Ship Monitoring, Damage Detection, Damage Visualization	Approved for public release; distribution is unlimited. Available from: National Technical Information Service Springfield, VA 22161 (703) 487-4650

19. Security Classif. (of this report)	20. Security Classif. (of this page)	21. No. of Pages	22. Price
Unclassified	Unclassified		

CONVERSION FACTORS
(Approximate conversions to metric measures)

To convert from	to	Function	Value
LENGTH			
inches	meters	divide	39.3701
inches	millimeters	multiply by	25.4000
feet	meters	divide by	3.2808
VOLUME			
cubic feet	cubic meters	divide by	35.3149
cubic inches	cubic meters	divide by	61,024
SECTION MODULUS			
inches^2 feet	centimeters^2 meters	multiply by	1.9665
inches^2 feet	centimeters^3	multiply by	196.6448
inches^3	centimeters^3	multiply by	16.3871
MOMENT OF INERTIA			
inches^2 feet^2	centimeters^2 meters^2	divide by	1.6684
inches^2 feet^2	centimeters^4	multiply by	5993.73
inches^4	centimeters^4	multiply by	41.623
FORCE OR MASS			
long tons	tonne	multiply by	1.0160
long tons	kilograms	multiply by	1016.047
pounds	tonnes	divide by	2204.62
pounds	kilograms	divide by	2.2046
pounds	Newtons	multiply by	4.4482
PRESSURE OR STRESS			
pounds/inch^2	Newtons/meter^2 (Pascals)	multiply by	6894.757
kilo pounds/inch^2	mega Newtons/meter^2 (mega Pascals)	multiply by	6.8947
BENDING OR TORQUE			
foot tons	meter tons	divide by	3.2291
foot pounds	kilogram meters	divide by	7.23285
foot pounds	Newton meters	multiply by	1.35582
ENERGY			
foot pounds	Joules	multiply by	1.355826
STRESS INTENSITY			
kilo pound/inch^2 inch^{½}(ksi$\sqrt{in}$)	mega Newton MNm$^{3/2}$	multiply by	1.0998
J-INTEGRAL			
kilo pound/inch	Joules/mm^2	multiply by	0.1753
kilo pound/inch	kilo Joules/m^2	multiply by	175.3

Table of Contents

List of Figures

List of Tables

1. Executive Summary

The U.S. Navy, Air Force, National Aeronautics and Space Administration (NASA) and other organizations have all contributed to the development of structural health monitoring sensors, data acquisition hardware, and techniques to process and interpret the resulting data for use on everything from civil infrastructure to space vehicles. One promising suite of sensors and data acquisition hardware, developed under multiple contracts with the U.S. Department of Defense and NASA, was recently licensed for commercial development and production. The purpose of the study detailed in this report is to take a first look at investigating whether the new commercial off-the-shelf structural health monitoring hardware is suitable for use on Navy surface vessels and, if not, to determine what improvements or modifications should be investigated for a maritime-ready health monitoring system capable of detecting defects in in-service ship structures.

Chapter 2 begins with a high-level, conceptual overview of how continuous ship structural monitoring fits into the concept of individual ship structure digital twins. As envisioned by the U.S. Navy, ship classification societies, and others in the maritime industry, these data, corresponding numerical models, and other information feed into a broader ship digital thread to enable a multitude of operator, maintainer, and engineering analyses. A brief introduction to structural health monitoring and the current state of monitoring surface ships is followed by an introduction to Lamb-wave damage detection techniques.

In Chapter 3 the technical details of both the commercial hardware and test structure are provided, along with sensor, hardware, and cable attachment procedures. Chapter 4 begins with a numerical wave propagation study, which serves as both a comparison for experimental wave propagation data as well as defining parameters in the test procedure for introducing damage events and acquiring experimental data. The algorithms and software to process the experimental results are described in Chapter 5, followed by a discussion of the detectability of the defects introduced to the structure. Finally, Chapter 6 contains a summary of the report's key findings and outlines a number of hardware and software improvements and future research.

2. Introduction

The maritime industry, along with much of the broader industrial, government, and academic community, is actively undertaking the Industry 4.0 paradigm shift, or "fourth industrial revolution". Advances in computing, big data analysis, artificial intelligence, digital twins, agile transformations, and related fields are enabling this “fourth industrial revolution,” where usage of large amounts of data provides previously unobtainable, real-time insights into numerous systems, processes, or assets. A large component of this digital transformation is the development and employment of digital twins.

For this study, we will consider a digital twin to be “an integrated multiphysics, multiscale, probabilistic simulation of an as-built vehicle or system that uses the best available physical models, sensor updates, fleet history, etc., to mirror the life of its corresponding [physical] twin” (Glaessgen and Stargel, 2012). For ship structures, one of the primary objectives of a digital twin is enabling both enhanced operational insights and condition-based maintenance. Digital twin implementation will ideally provide insight into real-time system health for individual assets. Each asset will have its corresponding twin, capturing differences in wear and tear across a class or fleet of ships. These insights allow for an assessment of the current state of health, allowing operators to predict expected future performance over a range of timescales.

While it is clear that the ongoing digital transformation is the future, the fact remains that many ship structures are physically large and highly complex. Defining an “as-built” structural model for a single ship is immensely difficult. Maintaining “as-is” or “as-operated” structural conditions for every ship within a classification program or a naval fleet is an even larger challenge. Automated assessments of ship structural usage and condition are key components to maintaining individualistic twins for every asset. Continuous structural health monitoring may provide one tool in maintaining accurate digital twins of ship structures.

For any number of structures, including civil, aerospace, and mechanical engineering infrastructure, structural health monitoring (SHM) is the process of implementing a damage identification strategy (Farrar and Worden, 2007). As opposed to the way one might think about the use of traditional nondestructive evaluation (NDE) techniques such as liquid penetrant inspection, magnetic inspection, eddy-current

inspection, radiography, or ultrasonic inspection to detect damage (Doherty, 1987), SHM methods are commonly performed while the structure is in use (Inman *et al,.* 2005). While NDE techniques generally require the system of interest to be inoperable, SHM can often be done in real time with algorithms and detection schemes finding changes to the structure almost instantaneously.

The obvious goal of any health monitoring application is to detect changes or damage to the underlying structure. Damage to typical monitored structures is defined as any change to the material, system geometric properties, boundary conditions, or system connectivity, which is either intentionally or unintentionally brought about. Usually, to be considered damage, these changes must adversely affect the current or future performance of the system (Doebling *et al.,* 1998; Inman *et al.,* 2005; Farrar and Worden, 2007).

Adams (2007) expands the definition of health monitoring to identifying four characteristics of a structure as it operates:

1. the operational and environmental loads acting on a structure
2. the mechanical damage caused by these loads
3. the growth of this damage during operation
4. the future performance of the structure due to cumulative damage effects

2.1 Ship Structural Monitoring and Digital Twin

SHM for ships, sometimes referred to as ship hull monitoring, is becoming more commonplace (American Bureau of Shipping (ABS), 2016; Drummen *et al.,* 2016; Hess, 2007; Salvino and Brady, 2007; Schiere *et al.,* 2017; Swartz *et al.,* 2010). In some cases, these installations are initiated with the primary directive to inform a ship structure digital twin. ABS is collaborating with the U.S. Navy's Military Sealift Command (MSC) to build digital twins for three vessels, with the goal of being able to practice condition-based maintenance instead of traditional time-based maintenance (ABS, 2018; Maritime Executive, 2018). Other studies have looked at building a ship structure digital twin with previously acquired full-scale or simulation data (Mondoro and Grisso, 2019; Drazen, *et al.,* 2019).

Effective hull structural monitoring systems provide effective information defining the operational and environmental loads necessary for SHM Characteristic 1 (Adams, 2007). The focus of research in this report is to concentrate on technologies addressing Characteristics 2 and 3 to detect, characterize, and track the growth of damage in ship structures. A combination of SHM Characteristics 1–4 is a ship structure digital twin. Continuously fusing the data with physics-based models and machine learning enables the prescription of multiple future instantiations of the ship and its environment and provides both operators and maintainers opportunities to identify optimum choices with a full understanding of current and future ship structural condition. The hardware under evaluation in this study could potentially be a primary source of data and information to update a structural digital twin.

2.2 Lamb Wave Monitoring

Guided waves, or Lamb waves, are ultrasonic waves which propagate in plate-like structures or materials where the plate thickness is comparable to the wavelength of the Lamb wave (Lamb, 1917). The waves propagate through the material thickness and are contained (guided) between parallel top and bottom surfaces. In analytical solutions to the Lamb wave propagation equations, two types of waves are revealed as valid solutions: symmetric and antisymmetric. For both wave types, a number of modes can exist, *e.g.*, S_0, S_1, S_2, etc. for symmetric waves. Complete details of Lamb wave propagation, including their use in structural health monitoring, analytical derivations, and interaction with specific materials or defects, are available in key texts by Achenbach (1973), Giurgiutiu (2014), Rose (2014), and others.

Lamb waves are a popular technique used by many in the structural health monitoring community (Giurgiutiu, 2014). A primary advantage of guided waves is the ability for waves to travel long distances in thin plates, which allows for monitoring of large areas with a relatively low number of transducers. Lamb waves are also easily excitable with piezoelectric actuators, which can be permanently adhered or embedded in structures. Guided-wave propagation signal analysis expands upon the fundamental understanding of wave propagation in structures established by the nondestructive evaluation community (Giurgiutiu, 2014). When using Lamb waves for structural health

monitoring, several features of the waveforms, including attenuation, scattering, or distortion, can be used for damage identification.

Two primary methods of data collection are typically utilized when conducting guided-wave experiments: pitch-catch and pulse-echo. Pitch-catch refers to a scenario with at least two piezoelectric transducers bonded to a structure. At any given time, one of the transducers acts as an excitation source while the other transducer(s) passively collect(s) the propagated wave signals. Damage in (or near) the path between the two transducers is discovered by monitoring data features such as wave group arrival delays or wave scattering. Alternatively, pulse-echo describes the technique were the same transducer that provides actuation also acts as a sensor. After an excitation signal is generated, the actuator (or one or more adjacent transducers) switches to sensing mode to record waves reflecting back to the source (echos) from edges or discontinuities in the material. Damage is detected in the form of new reflections or modified waveforms and understanding of the time-of-flight of the propagating wave modes. Both pitch-catch and pulse-echo methodologies will be utilized in this study.

2.3 Commercial SHM Solution

The primary intent of this effort is to investigate the practical use of the commercial off-the-shelf (COTS) SHM sensors and data acquisition hardware for damage detection in representative ship structure. The targeted technology is a guided-wave SHM system developed by Metis Design Corporation under multiple Small Business Innovation Research (SBIR) and Small Business Technology Transfer (STTR) programs with the U.S. Navy, Air Force, NASA, and others. The technology is exclusively licensed for commercial production by Collins Aerospace, formerly United Technologies Aerospace Systems (Collins Aerospace, 2016). A further description of the COTS SHM hardware will be provided in Chapter 3.

2.4 Research Goals

Although SHM sensor development has been an active area of research for many years, ruggedized, COTS SHM systems that have proven effective and validated in relevant maritime operational environments are generally limited to the collection of

ship strain or acceleration data. These systems are typically not capable of detecting damage before it grows to a potentially problematic magnitude. Previous studies by this author revealed the ability of active SHM techniques to detect damage in relevant ship construction materials and structures (Grisso *et al.,* 2011a; Grisso *et al.,* 2011b; Grisso, 2013). However, the conducted research and design processes revealed the perceived benefits of utilizing COTS products as opposed to the often-tedious administrative burden of developing technology solutions in house. The testing proposed here looks to build upon previous maritime SHM studies to determine if active damage detection techniques are suitable for inclusion in larger shipboard health management systems. The following chapters describe the COTS SHM hardware in more detail, introduce the subject test structure and data collection processes, and describe the data analysis techniques and results. Chapter 6 wraps up the report with a list of key findings and recommendations for appropriate future work.

3. SHM Hardware and Experimental Structure

3.1 COTS Hardware Overview

The Collins Aerospace MD7-Pro digital structural health monitoring system consists of three primary components: the accumulation node, the acquisition node, and the sensor base, or structural sonar. A key feature of the system is fully digital data acquisition. The MD7-Pro system is networked on a serial bus for power, command, data transfer, and synchronization. Data is digitized at the measurement location, which eliminates susceptibility of the data to electro-mechanical interference (EMI) resulting from long analog cable runs and reduces the overall cabling and hardware footprint required for a distributed sensing installation (Metis Design Corporation, 2019).

When considering the entire MD7-Pro SHM system as analogous to the human nervous system, the accumulation node is the brain of the hardware. The accumulation node, measuring 2.4 x 1.6 x 0.2 inches and weighing less than 1 ounce, is the primary controller and interface relaying commands to the acquisition nodes. An accumulation node runs on 28 V_{DC} and can support 24 acquisition nodes. The accumulation node contains 8 GB of internal static memory, a field-programmable gate array (FPGA) with an ARM processor, and 16 digital input channels (Metis Design Corporation, 2019).

The spine of the MD7-Pro system is the 2.0 x 1.6 x 0.2 inches, 0.6-ounce acquisition node. The acquisition node provides the primary data acquisition functionality of the system, replacing bulky, centralized data collection hubs, servers, or computers. The acquisition node provides up to a 20-V_{PP}, 20-MHz analog actuation signal to the attached sensor base actuator, while simultaneously measuring six 12-bit channels at sampling speeds up to 50 MHz. Two GB of internal memory allows for temporary local data storage, and integrated internal temperature and acceleration measurements provide additional monitoring capability. Both the accumulator and acquisition nodes are potted in urethane to provide resistance to moisture, chemicals, fire, and shock exposure. In addition to the six high sampling rate channels, the acquisition nodes can also acquire additional external, differential voltage sensor signals, such as temperature, acceleration, strain, etc. (Metis Design Corporation, 2019).

Finally, the structural sonar containing piezoelectric transducers act as nerves mating with the acquisition or accumulation nodes to provide a number of sensing inputs. The sensor bases bond directly to the structure of interest, similar to a typical strain gauge. The nodes then attach over the bonded sensor bases to provide both protection to the transducers and electrical connectivity. While a number of sensing nodes exist for different measurements, this study will focus solely on the MD7-Pro structural sonar. The structural sonar contains one central piezoelectric actuator and six piezoelectric sensors in a single enclosed package. The array of sensors provides both active and passive beamforming to passively detect impact or acoustic emission events or to actively perform guided-wave interrogation. The active technique allows for the generation of spatial damage maps indicating the probability of damage across the structure due to localized changes in stiffness. Similarly, passive beamforming can pinpoint the source location of impact or acoustic emission events such as crack growth (Metis Design Corporation, 2019). The MD7-Pro components can be seen in Figure 1.

Figure 1. The MD7-Pro structural sonar (left), acquisition node (center), and accumulator node (right)

The MD7-Pro components are connected with preassembled and wired connectors from Omnetics Connector Corporation. The dual row, rectangular connectors are intended for use in very densely packaged electronic components and fully digital applications. Wires and contacts are precrimped and potted during manufacturing, and they are mated with finely threaded (0-80) screws and prethreaded mounting holes to reduce susceptibility to vibration loosening. The connectors and cables are assembled in a Military Standard [MIL-STD]-790 approved manufacturing facility and meet the requirements detailed in Military Detail Specification [MIL-DTL]-32139, including insulation resistance, temperature cycling, humidity, vibration, mechanical shock, salt spray contact resistance, retention, thermal outgassing, etc. (MIL-STD-790, 2018; MIL-DTL-32139, 2017). Once assembled, the accumulation node provides the communication and protocol for interaction with the rest of the system. In the past, procedures have been developed to marinize the MD7-Pro components for operation with exposure to seawater as well as extended submersion and hydrostatic pressure (SBIR Topic N111-053, 2011; Metis Design Corporation, 2013).

As Figure 2 shows, the accumulation node can be connected to a host device via either Ethernet or a serial port. In general, each accumulator node can support a digital bus of up to 24 acquisition nodes with cable lengths up to 30 m. Power is supplied to the accumulation node and distributed across the digital bus to the acquisition nodes. The number of nodes and length of the bus is not a fixed number and depends upon the voltage drop along the span of the bus. The accumulator node can operate autonomously with defined acquisition programs, such as collecting data twice daily, or remotely operated via wired or wireless protocols. The MD7-Pro structural sensing components can integrate within a larger health and usage monitoring system (HUMS); however, only the structural portion is evaluated in this study.

Figure 2. The MD7-Pro bus assembly prior to structural sonar attachment

3.2 Test Structure Instrumentation

The structure used for demonstrating the SHM hardware is a welded steel grillage measuring 24 x 8 ft. The grillage has both welded steel longitudinal and transverse stiffeners to represent typical ship deck plating with 6-foot frame spacing. Figure 3 shows the dimensions of the grillage structure, along with the locations of the acquisition nodes. The structure has welded end platens and side plates, which allow the specimen to bolt into the Naval Surface Warfare Center, Carderock Division large grillage test machine. Deck plating is ¼-inch or 5/16-inch A36 steel, butt welded in the center bay.

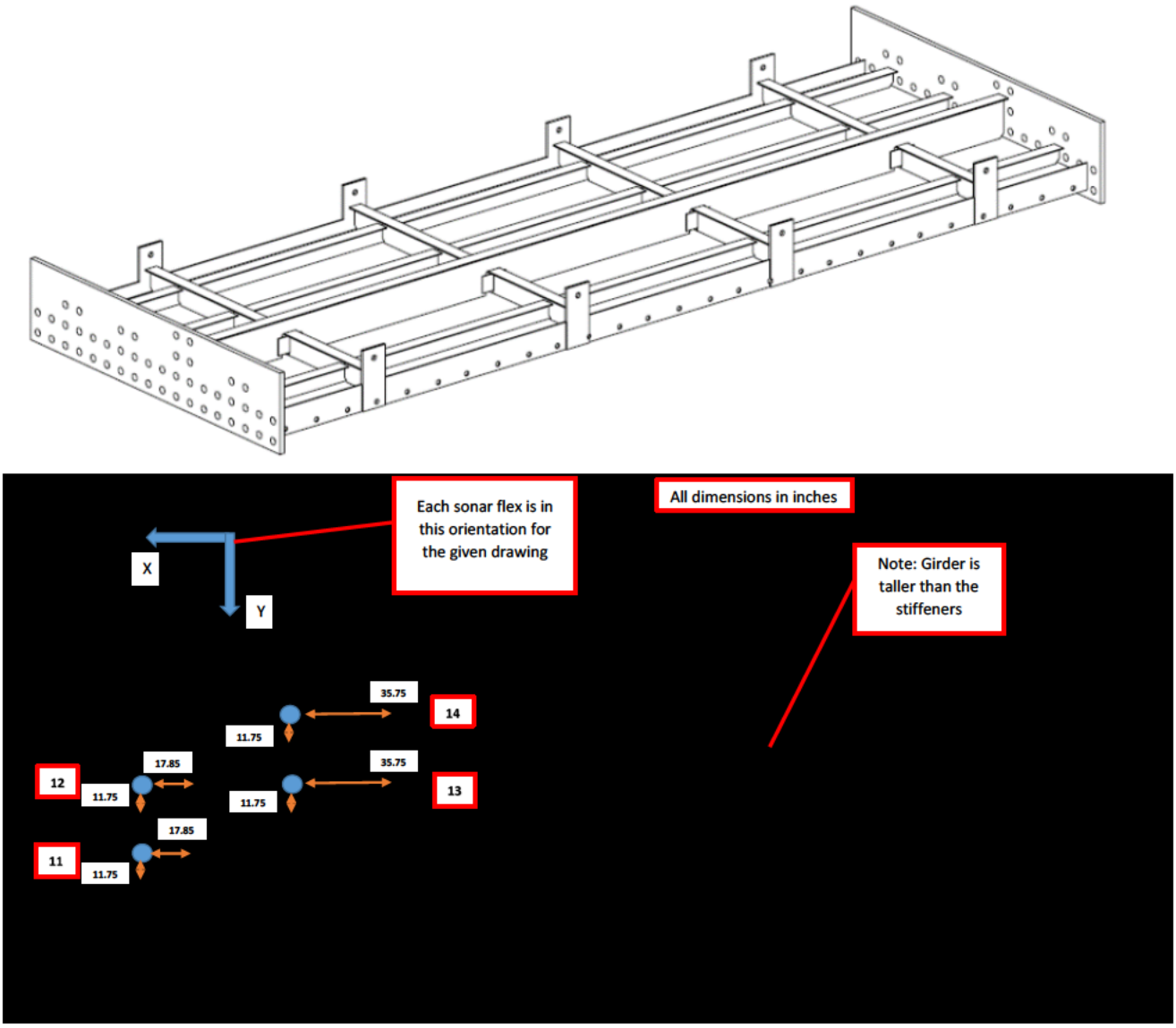

Figure 3. Isometric view (top) and dimensioned (bottom) diagrams showing dimensions of the grillage structure with the MD7-Pro acquisition node locations identified

Acquisition nodes are individually numbered to allow programming and control via the accumulator (ACC) node. The acquisition (ACQ) nodes used in this study are numbered 11–14. Before attaching the ACQ nodes to the bonded structural sonars, the entire bus was assembled in an office setting to enable programming of the data acquisition nodes and to ensure electrical connectivity across the bus. To cover the grillage layout, the ACQ nodes are configured in left (ACQ 11 and ACQ 12) and right (ACQ 13 and ACQ 14) sides of the bus. To the left in Figure 2 is the ACC node Ethernet and power adapter.

Four ACQ nodes were purchased to support these experiments, so four structural sonar arrays were installed at the locations identified in Figure 3. As mentioned, the sensor base installation process mimics that of a strain gauge, with the primary difference being the availability of a structural sonar installation tool. The installation tool (Figure 4) is used to apply consistent pressure to the sensor base as the adhesive cures. The tool can pick up a structural sonar directly from its shipping packaging, which avoids contamination of the bonding surface, and locks the sensor base into place for installation via a latching mechanism. The tool then attaches to the structure via releasable double-sided tape. Figure 5 shows an example of sensor installation. Brief steps for applying a sensor base are as follows:

1. Mark the target installation with x- and y-axis crosshairs.
2. Sand the base installation area with medium-grit sandpaper.
3. Clean the installation area with alcohol or acetone and a nonpilling wipe; remark the crosshairs as necessary
4. Pick up the structural sonar in the installation tool, noting the positive x- and y-directions, and secure it into place with the latch.
5. Apply a thin, uniform layer of strain gauge adhesive (Vishay Micro-Measurements AE-10 or similar) to the back of the sonar.
6. Remove the backing of the double-sided tape, double checking the x- and y-axes, and press the installation tool onto the structure until the tape is securely bonded (approximately 1 min).
7. Press down on the center of the tool to engage the bonding pressure.
8. Once curing is complete, unlatch the lock holding the sensor in the tool, and remove the tape to release the tool.

Figure 4. Top, side, and bottom views of the structural sonar installation tool

Figure 5. Sensor installation tool holding the sensor base for ACQ 11 in place for the cure cycle (top) and area marked and prepared for installation of ACQ 12 (bottom)

As shown in Figure 1, the structural sonar has white markings on the outer Kapton (polyimide film) protective layer outlining where the edge of the ACQ node should sit. Also indicated are lock and unlock symbols. The circuit board of the sensor also has different shaped tabs along the outer diameter, which help to prevent misalignment of the ACQ node. To install the ACQ node onto the sensor base, one

should align the node with the outline and tabs and then rotate the node 90° clockwise to secure the node to the base. Once the node is attached to the sensor base, the cables are fastened to the ACQ nodes in the desired bus configuration. Figure 6 and Figure 7 show the installed nodes and cables.

Figure 6. ACQ 11 (bottom) and ACQ 12 attached to the sensor bases with cables installed

Figure 7. A view of the test setup, including the data acquisition laptop (note that picture is flipped 180° from the rest of the pictures and layout)

4. Data Acquisition

4.1 Numerical Wave Propagation

As previously noted, Lamb waves propagate in symmetric and antisymmetric types, with a number of modes existing for each case (*e.g.*, S_0, S_1, S_2, etc. for symmetric waves). Numerical solutions exist to predict wave propagation in different materials and simulate the interaction of propagating waves exposed to various types of damage (Giurgiutiu, 2014).

Guided waves are often described via dispersion curves, which plot wave mode speed in a given material as a function of frequency or the frequency thickness product. In essence, the dispersion curve reveals what modes may be present at any given excitation frequency and how quickly those modes propagate through the structure. Using freely available software (Waveform Revealer 3), Figure 8 displays the theoretical group velocity dispersion curve for ¼-inch A36 steel. Another useful plot to understand Lamb waves and their interaction with materials and defects is frequency versus wavenumber, which is the inverse of the wavelength. As shown in Figure 9, for any given excitation frequency, there could be a large separation in wavelength of the propagated modes. Different wavelengths and dispersion properties of modes leads to different interactions of each mode type with similar defects.

Now that we have an idea of what Lamb wave types and modes may be present at different actuation frequencies, as well as their wave speed and wavelength, let us continue with a numerical simulation of guided waves propagating in our target structural material. We know from Figure 8 that, under 250 kHz, we are likely to excite only the S_0 and A_0 modes (and perhaps a Rayleigh surface wave). We also know that the S_0 mode should travel at a significantly higher velocity through the structure than A_0. Knowing this, we can simulate a wave propagating through our target material of ¼-inch-thick A36 steel. Figure 10(a) shows an infinite plate with a bonded piezoelectric actuator and sensor placed approximately 20 inches apart. The actuator is excited with five cycles of a 160-kHz Hanning-windowed sine wave Figure 10(b). The Hanning-windowed, single-tone burst is a typical excitation used for propagating Lamb waves. In Figure 10(c), we can see the arriving waves recorded at the sensor. The S_0 and A_0

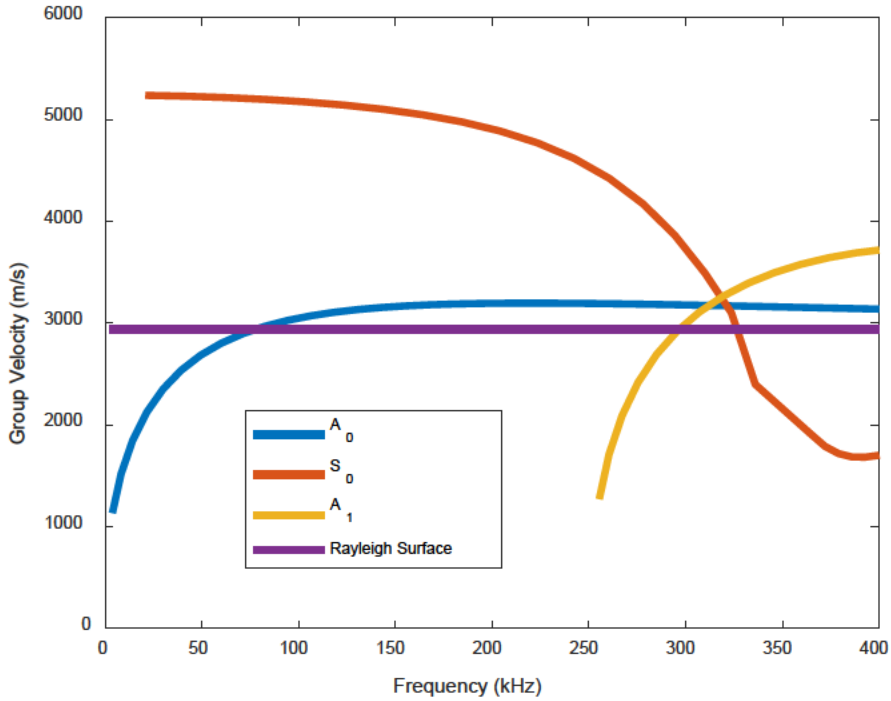

Figure 8. Group-velocity-versus-frequency dispersion curves in ¼-inch A36 steel

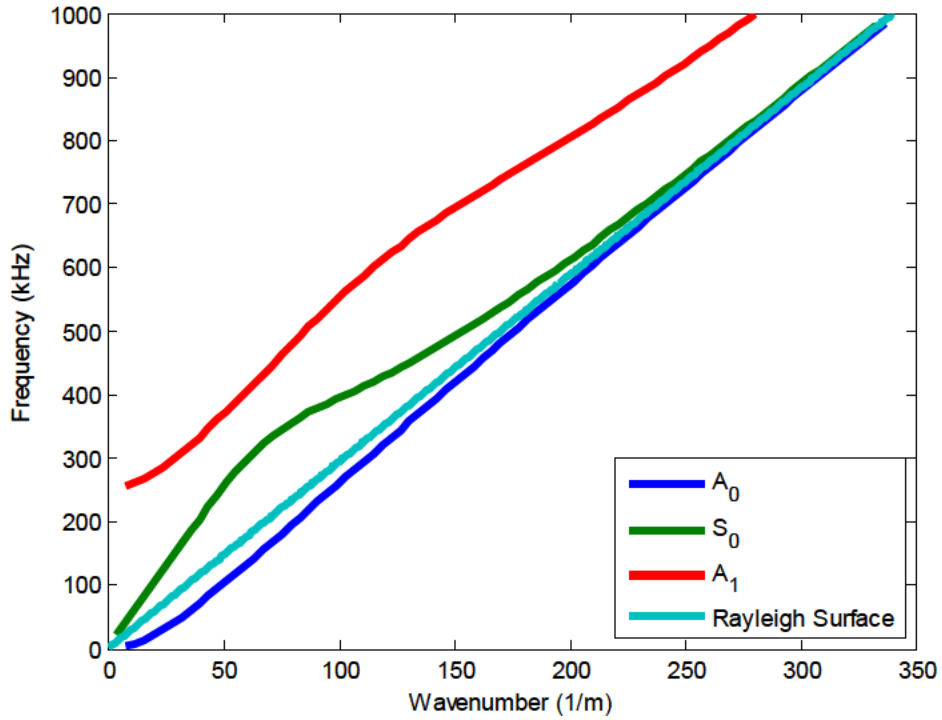

Figure 9. Frequency-versus-wavenumber dispersion curves in ¼-inch A36 steel

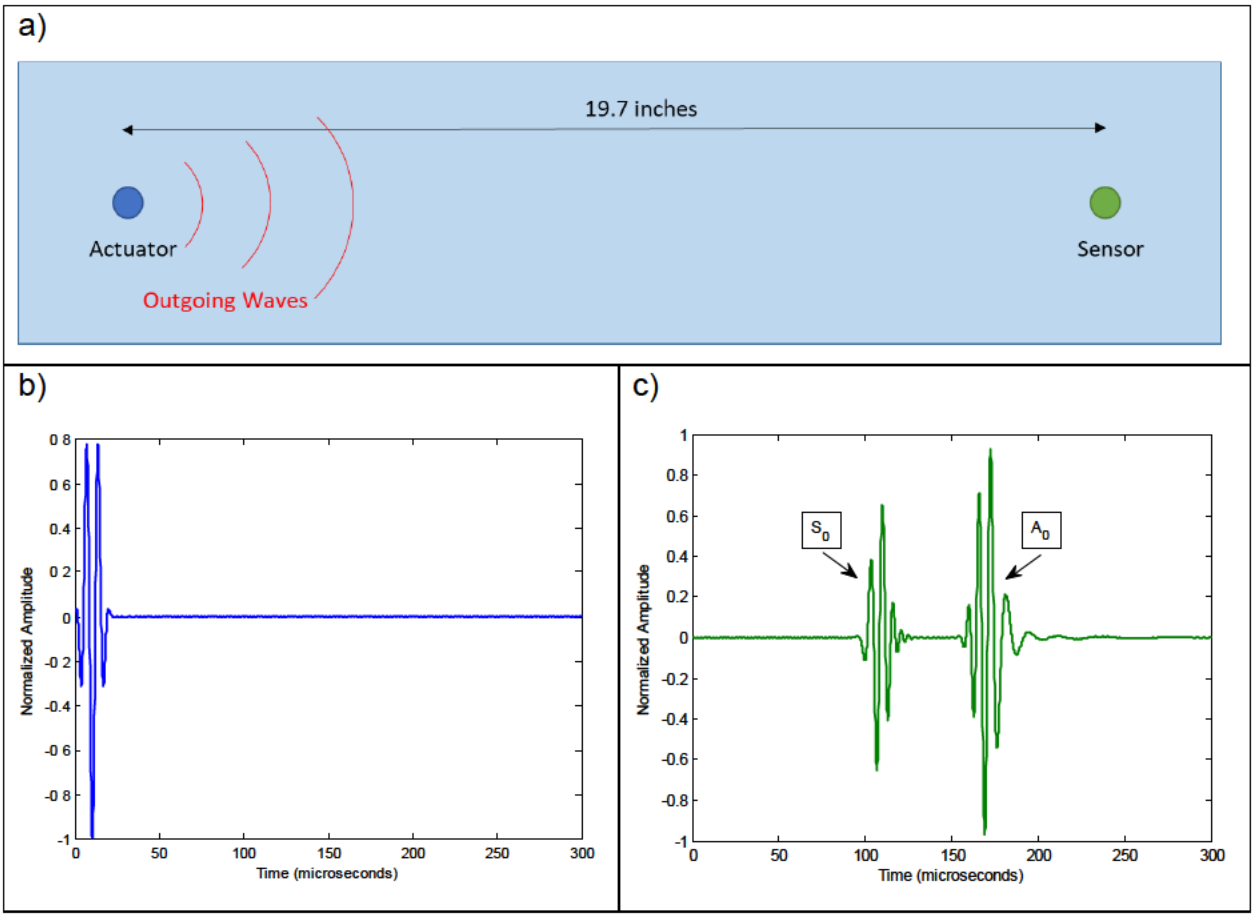

Figure 10. Simulated infinite plate of ¼-inch-thick A36 steel with bonded piezoelectric actuator and sensor (a), the actuator excitation signal (b), and waveforms recorded at the sensor (c)

mode arrivals are temporally separated and, thus, readily distinguishable. As expected, the S_0 wave package arrives earlier than A_0.

Now, let us use the same setup and simulate what happens when damage is introduced to the material. As shown in Figure 11(a), a small defect is introduced halfway between the actuator and sensor. The damage will cause the propagating waves to modify. Waves will reflect back toward the actuator after interacting with the defect. The damage also causes alterations to the original outgoing waveforms, which would induce waveform changes in the measured sensor signal.

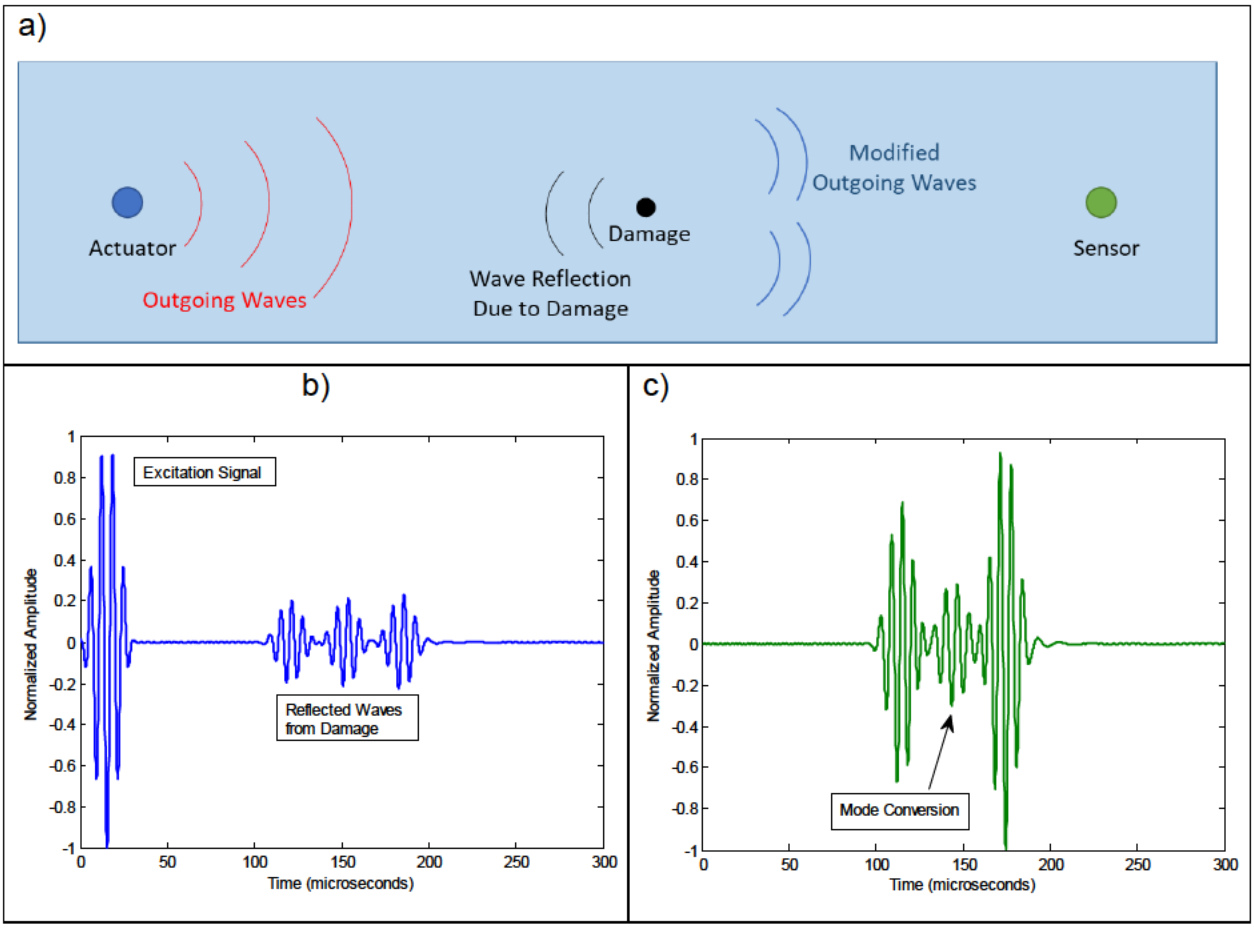

Figure 11. Simulated infinite plate of ¼-inch-thick A36 steel with damage between the piezoelectric actuator and sensor (a), the actuator excitation signal (b), and waveforms recorded at the sensor (c)

In Figure 11(b), we can see that, beginning around 100 μs, there are wave packets arriving back at the actuator location. These waves, which do not appear in Figure 10(b), are reflections from the damage. Similarly, there are slight phase and amplitude changes to the waveforms at the sensor seen in Figure 11(c). There is also a new mode, caused by mode conversion (e.g., A_0 mode converting to S_0, or similar) due to the presence of a defect. Note that the mode conversion and other parameters are indicative of a small defect, but not necessarily representative of a specific type of damage. Figure 12 shows the comparison between the baseline and damage waveforms as an illustrative example of the type of change to signals that may occur due to interaction with a new or growing defect. With this understanding of how waves may propagate in our structure, the experimental data acquisition parameters are established.

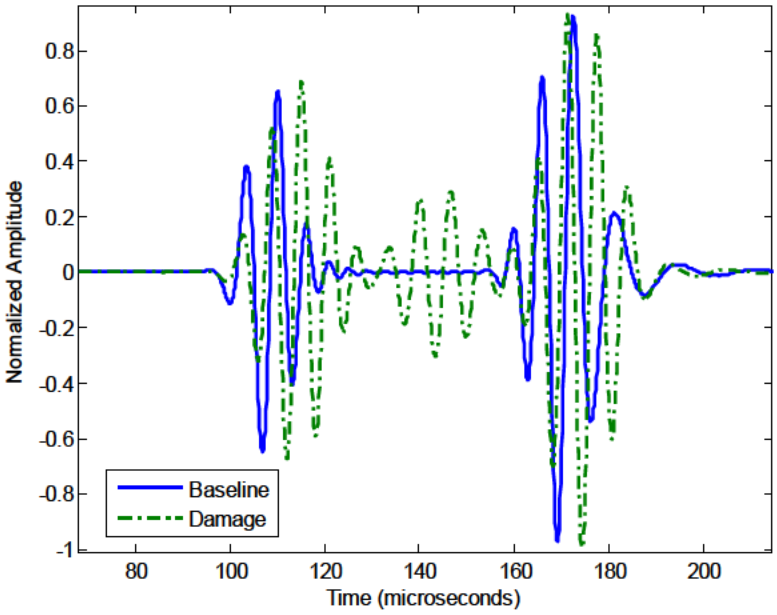

Figure 12. Simulated baseline and damage waveforms recorded by the sensor

4.2 Data Acquisition Directories and Functions

When setting up the data acquisition of the MD7-Pro system, there are two communications protocols: Ethernet and serial. In this case, an Ethernet connection to a host computer is utilized. To facilitate communication with the ACC node, a series of Command Prompt Interface (CMD) tools are included with the MD7-Pro hardware. The CMD Tools are standalone executable files which are initiated via a Windows operating system standard command prompt (Collins Aerospace, 2018). Once the ACC node is connected to a host computer through an open Ethernet port, a static internet protocol (IP) address compatible with the IP address of the ACC node must be established. A user may then login to the ACC node. A series of standard functions, such as “Upload”, “Download”, and “Sync,” allow the transfer of files or directories between the ACC node and host computer.

In addition to the CMD tools, a second set of standalone executables called Host Interface (HI) tools define the parameters of ACQ node data acquisition. Host interface tools act as standalone commands or as a group of subroutines under higher level programs. Notable tools include “HI_Discovery,” which allows a user to discover which ACQ nodes are properly connected to a bus, “HI_Sys_Status,” which provides a system status display to the host computer, and “Hi_List,” which builds a visual directory tree of

the ACC node and displays the results onto the host computer console. “HI_Test_Start” and “HI_Test_Stop” commands may start or end one or more of the programmed tests uploaded onto the ACC node (Collins Aerospace, 2018).

The ACC node directory structure defines specific data acquisition parameters. To execute a data collection event, specific files must be loaded into three main directories: “Tables,” “Modes,” and “Profiles.” The “Tables” directory stores files which define sequential commands to execute for a single data acquisition program. A “Modes” directory contains files that define individual tests, such as an active guided-wave test or a passive acoustic emission test, within a run file of the table directory. Finally, the “Profiles” directory is used to define individual test parameters. Collected data is stored in a “Results” directory, which can be downloaded to the host computer via the CMD Tools “Download” executable (Collins Aerospace, 2018).

Example code and files within the directory structure are available in Appendix A. When looking at the files, note that the “Table” or execution profile calls on the “Modes.” The “Modes,” or types of measurement to be collection from each individual node, then rely on the “Profiles” to define the specific parameters for each test, such as signal gain, excitation voltage, etc.

4.3 Damage Cases and Data Collection

The ACQ node arrangement on the grillage aims to detect damage over a large spatial area. As such, the damage induced to the structure will be a mix of locations and damage types, which may be easily detectable or, conversely, on the fringe of detectability. The first damage is a ¼-inch-diameter through-hole that should be in the pitch-catch path between ACQ 13 and ACQ 14. The rest of the damage cases are simulated cracks at welds or in the baseplate. Table 1 contains the damage labels, their location, and nearest ACQ node, while Figure 13 plots the ACQ nodes and damage locations. Damage 1 and ACQ 13 are shown in Figure 14. Figure 15 displays a sample crack in the weld toe of a longitudinal stiffener, corresponding to Damage 3. Pictures of the remaining damage cases are contained in Appendix B.

Table 1. The grillage damage case descriptions

	Location (x, y) (in)	Damage Description (in)	Nearest ACQ Node
Damage 1	(68.3, 57.3)	¼ diameter through hole	ACQ 13
Damage 2	(108.0, 55.1)	1 long crack (rotary tool cut)	ACQ 13
Damage 3	(78.5, 60.0)	1 long crack (rotary tool cut)	ACQ 13
Damage 4	(56.3, 65.0)	1 long crack (rotary tool cut)	ACQ 14
Damage 5	(37.0, 71.4)	1 long crack (rotary tool cut)	ACQ 14
Damage 6	(12.2, 41.6)	1 long crack (rotary tool cut)	ACQ 12

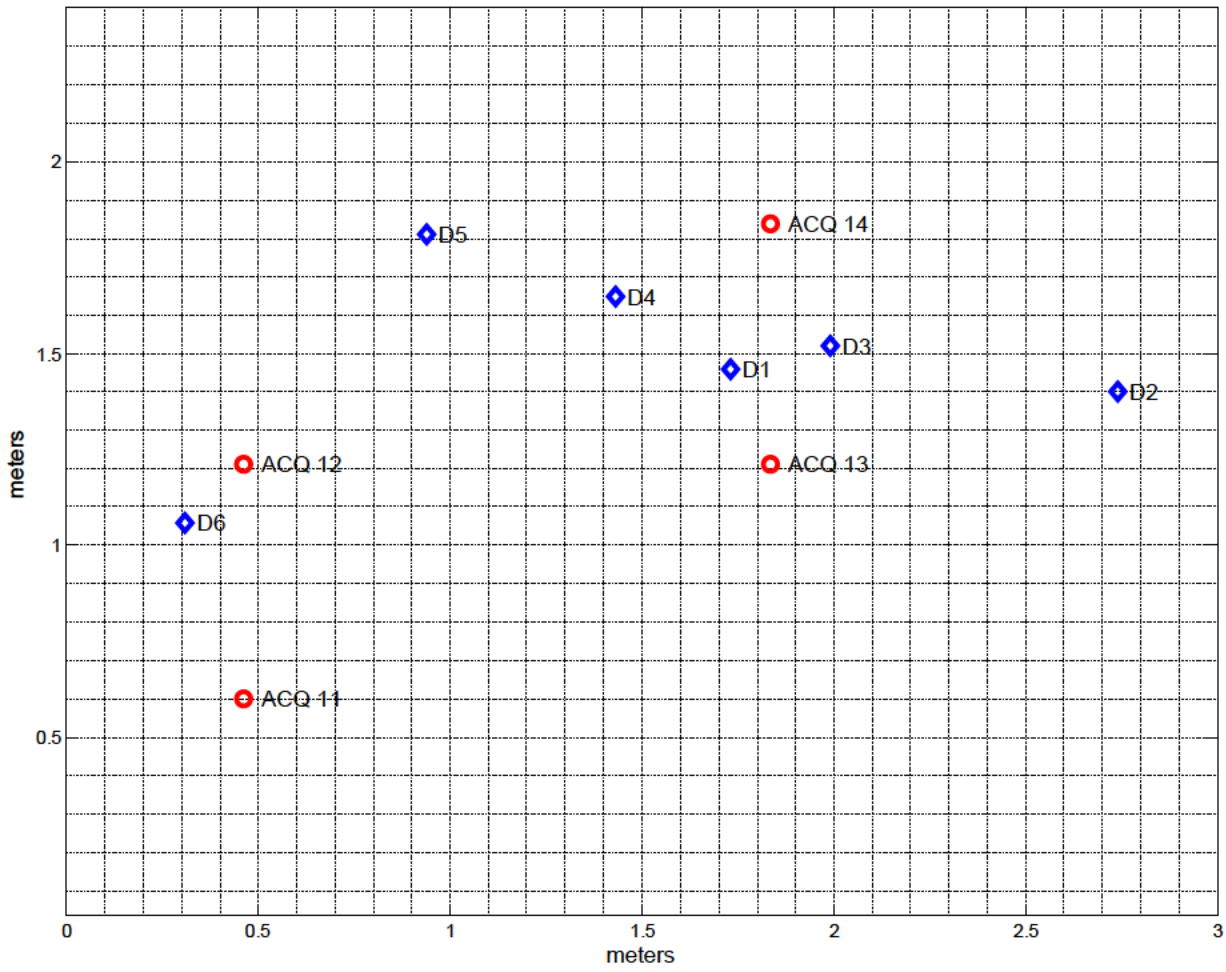

Figure 13. The locations of the ACQ nodes and six damage cases

Figure 14. Damage 1, a 1/4-inch through-hole, shown in relation to ACQ 13

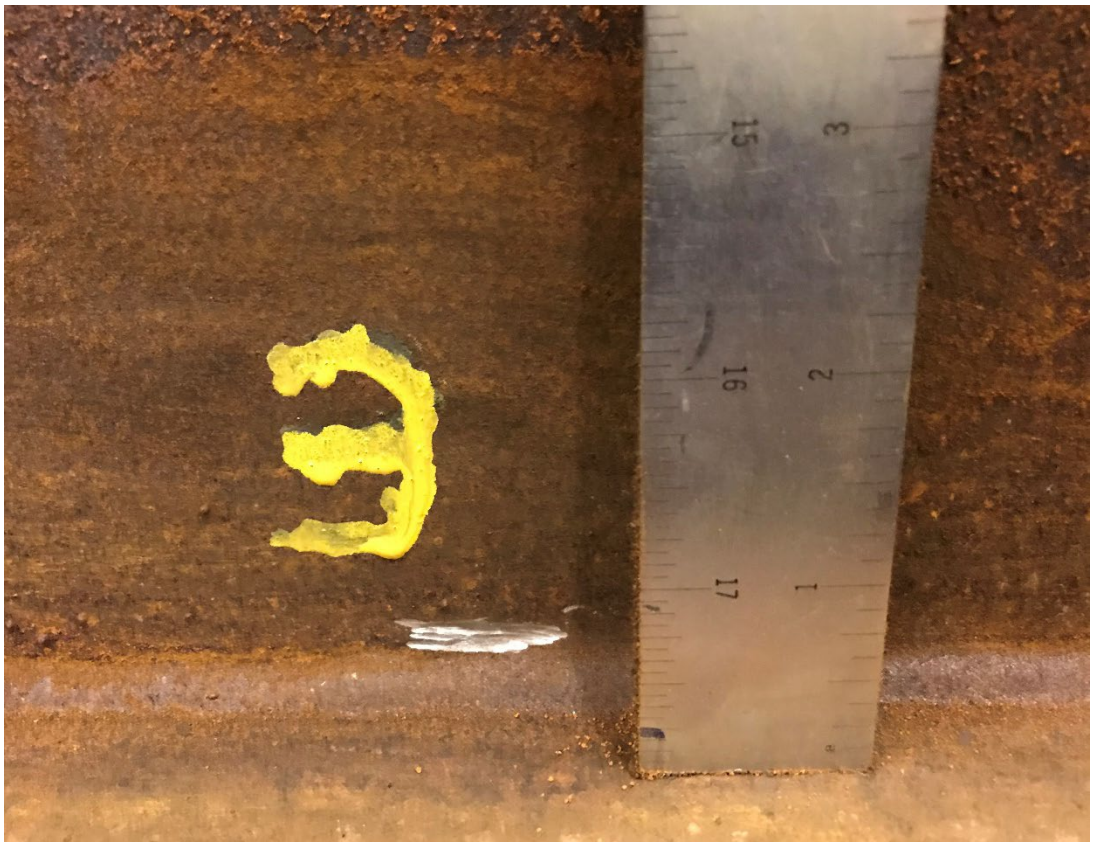

Figure 15. Damage 3, a simulated crack at a longitudinal stiffener weld toe

To induce wave propagation, a chirp actuation signal from one of the ACQ nodes is applied to the structural sonar actuator. The chirp provides a range of structural input from 50 kHz up to 300 kHz. The chirp signal is a linear sine sweep occurring over a period of approximately 100 μs (Figure 16). The actuation voltage is 20 V peak-to-peak. Data on all channels are recorded with 10-MHz sampling over a period of 1000 μs, yielding 10,000 samples for each channel per test. Each recorded test consists of 512 averages. The test setup and data acquisition parameters detailed in Appendix A remained constant for each damage case. At least three baseline data sets were used for reference for each of the test cases, and at least two full data sets were collected after every damage step.

4.4 Experimental Wave Propagation

In Figure 16, we see the chirp excitation signal from the actuator piezoelectric transducer in the center of the ACQ 13 structural sonar. The relative size and position

of the actuator can be seen in Figure 17. Looking at the sensors in the same sensor base, we can see our first indication of how waves are propagating in the grillage structure. Figure 18 displays the recorded sensor signals from ACQ 13. Due to the close spatial proximity of the actuator and signals, the waves arrive nearly instantaneously.

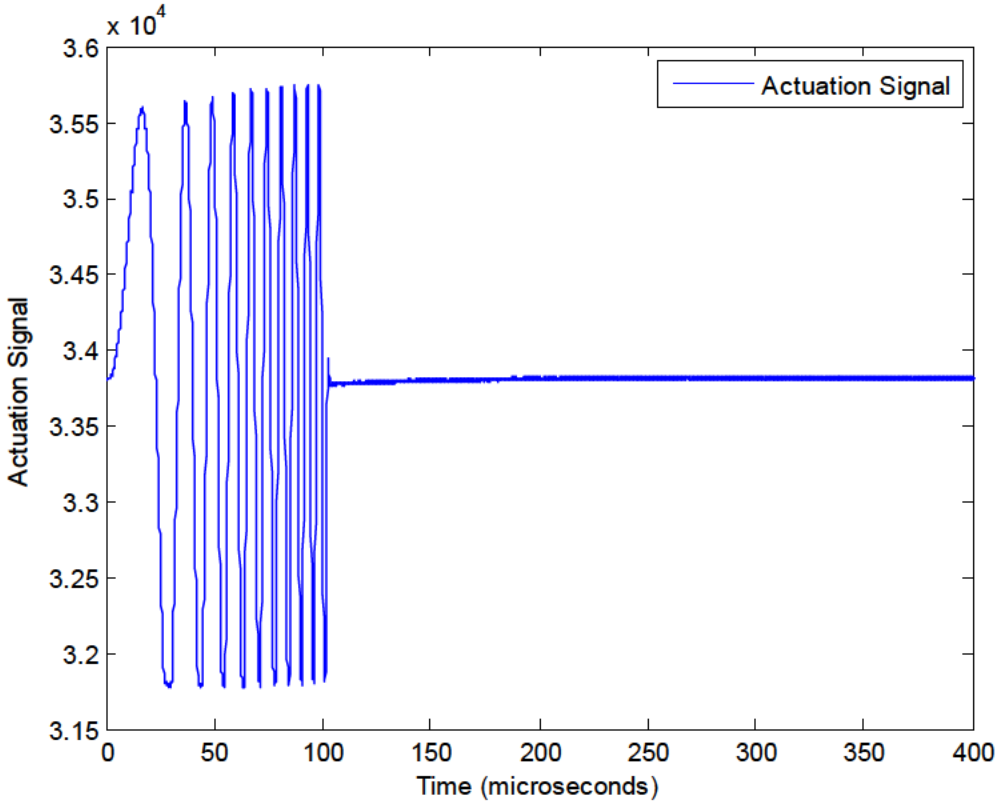

Figure 16. A swept sine, or chirp, signal used for guided-wave excitation recorded from the ACQ 13 actuator channel

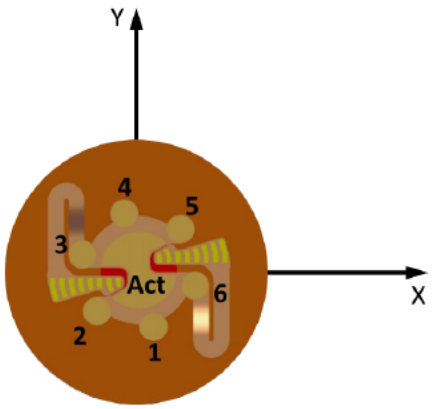

Figure 17. The orientation of the central actuator and six sensors in the structural sonar sensor base

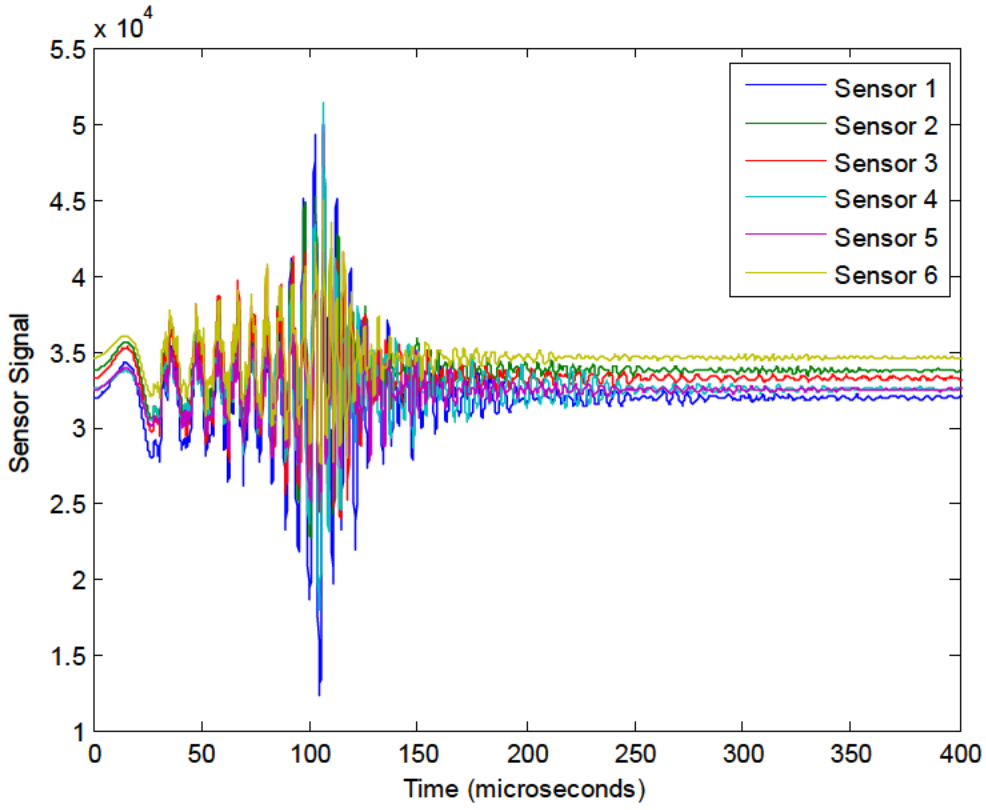

Figure 18. ACQ 13 sensor signals showing outgoing wave propagation

Except for some DC offset, the signals seen in Figure 18 are nearly identical, as would be expected with a homogeneous metallic plate. The sensors are not spatially distant enough from the actuator for the different types and modes of Lamb waves to separate. However, when we look at the sensor data received at ACQ 14 (Figure 19),

we can see more separation in the propagating waveforms at varying amplitudes and frequencies.

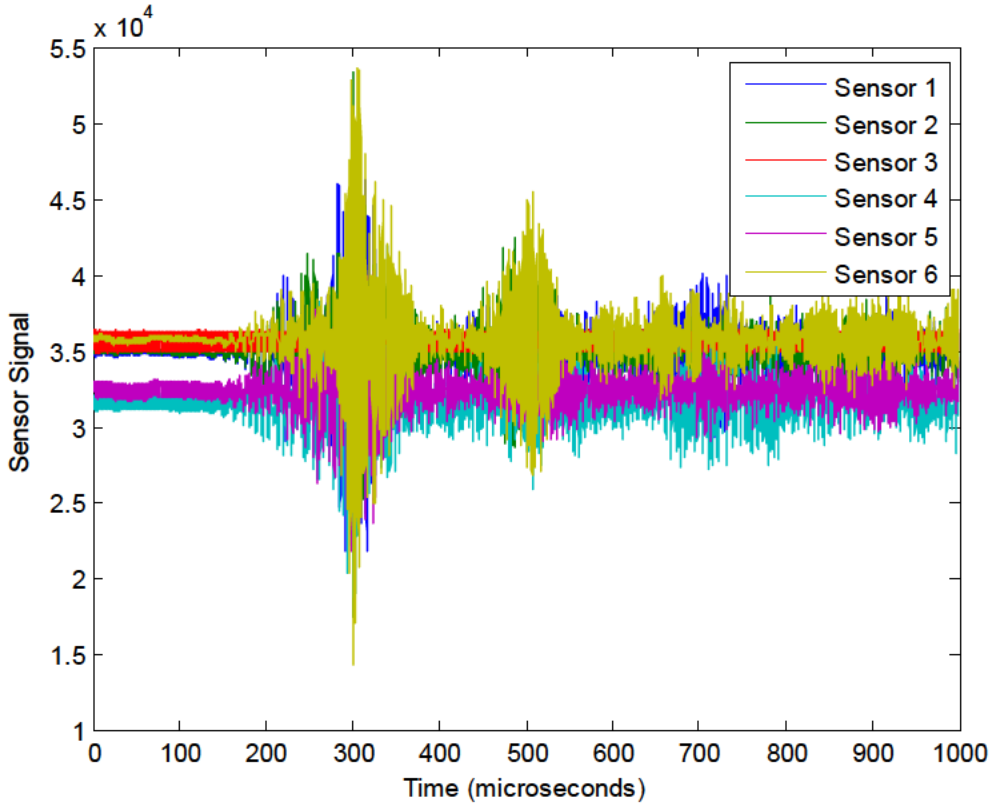

Figure 19. ACQ 14 sensor signals showing received waves from the ACQ 14 actuator

Figure 19 reveals numerous wave packets arriving shortly after 150 μs and continuing to the end of the sample period. Since we are exciting both S0 and A0 modes in a range of frequencies, wave speeds, and wavelengths in short proximity, visual identification of separate modes is difficult. However, we are still able to discern slight changes in the arriving signals due to damage.

In Figure 20, we see received wave data recorded from sensor Channel 4 of ACQ 14. Single traces from baseline, or healthy, data and post-Damage-1 data show minor shifting of the waveform signal. Channel 4 refers to the fourth sensor shown in Figure 17. Though the differences are subtle, a plot of the residuals (Figure 21) between the two signals shows that we do, in fact, have changes in the signal due to the ¼-inch hole. Each trace is averaged 512 times, so even minute received waveform differences are used to extract damage information. From this point forward, it will be

more illustrative to look at processed data instead of raw time histories. The following section will briefly describe the data processing techniques and the options and parameters available to extract significant features from the complex time series datasets.

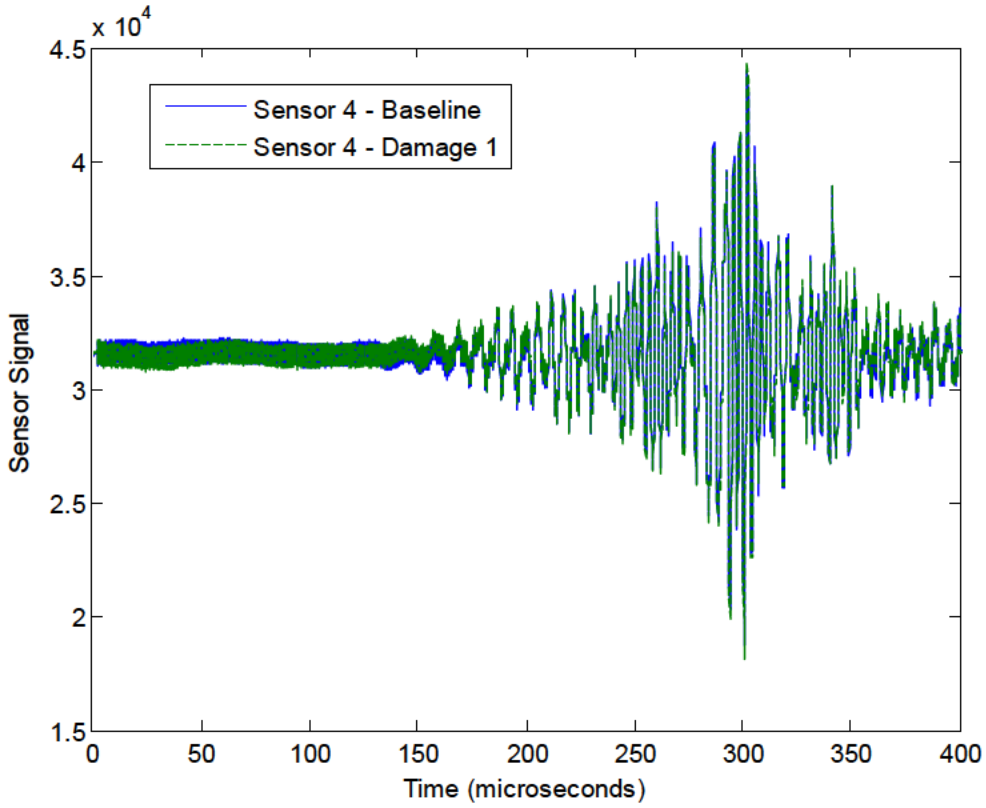

Figure 20. Baseline and Damage 1 waveforms recorded on sensor channel 4 of ACQ 14 (excitation is from ACQ 13)

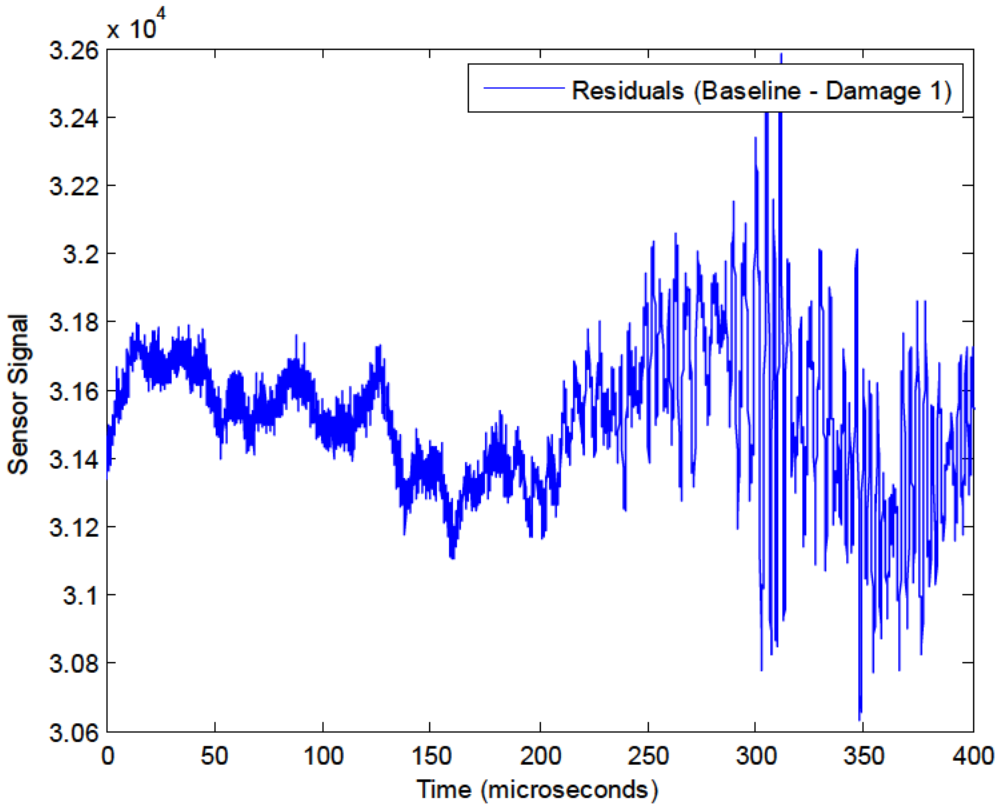

Figure 21. Residuals of the data from Figure 20

5. Data Analysis

Data acquisition utilizes a chirp function to excite a broad range of frequencies, which greatly aids in minimizing acquisition setup time. A chirp eliminates much of the tuning typically necessary for finding the excitation frequencies with the best propagation properties, signal-to-noise ratio, sensitivity to damage, etc. Interrogating the structure with a broadband excitation also assists with reducing the time necessary to acquire data. However, processing the data involves reconstructing a narrowband signal from the broadband data. The processing software allows the user to choose the individual frequencies of interest to analyze, knowing that data from 50 kHz to 300 kHz is recorded and available for examination.

To analyze the data, a hybrid beamforming technique is used. At each individual node, incoherent beam forming creates combined images from each sensor. Across all the nodes, coherent beamforming combines spatial damage information from the individual nodes. The combined images, with imposed logic to account for boundary conditions, line-of-sight issues, etc., can then reveal location damage and severity. Matching pursuit algorithms identify scatter targets. Full details of the data acquisitions, signal conditioning, and damage detection algorithms developed by Metis Design Corporation are described in several papers (Flynn *et al.*, 2011; Jarmer *et al.*, 2014; Kessler *et al.*, 2011a and 2011b).

To generate the damage identification maps, a meshed model must first be imported into the software (Figure 22 and Figure 23). For this study, the three-dimensional (3D) geometry is imported, but analysis will be limited to the two-dimensional baseplate. ACQ node locations are imported and placed on the structure in same locations as the physical structure.

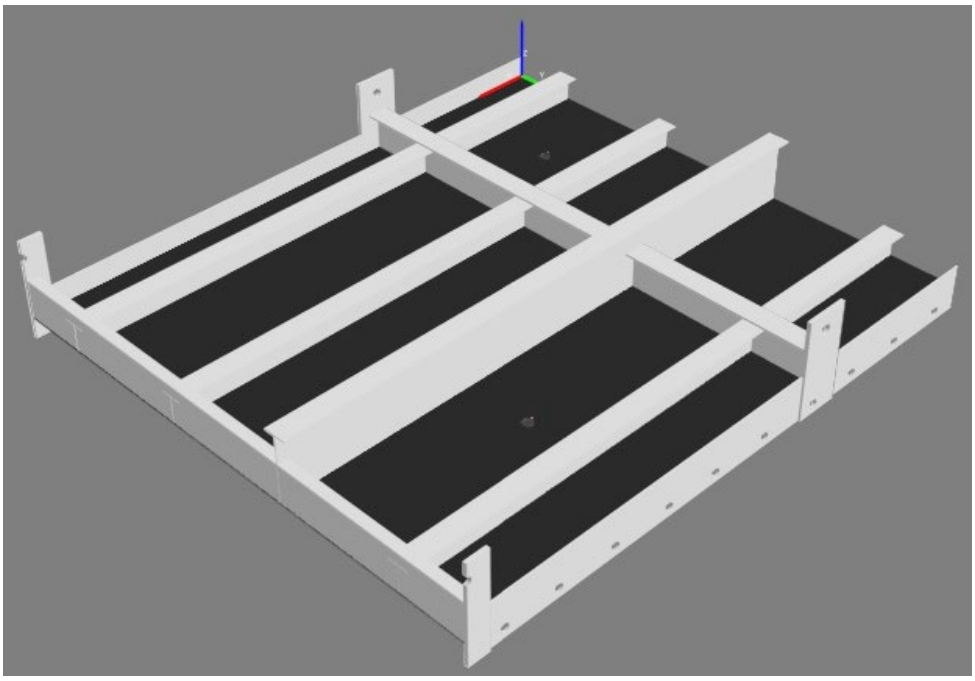

Figure 22. An isometric view of the grillage structure used for data processing

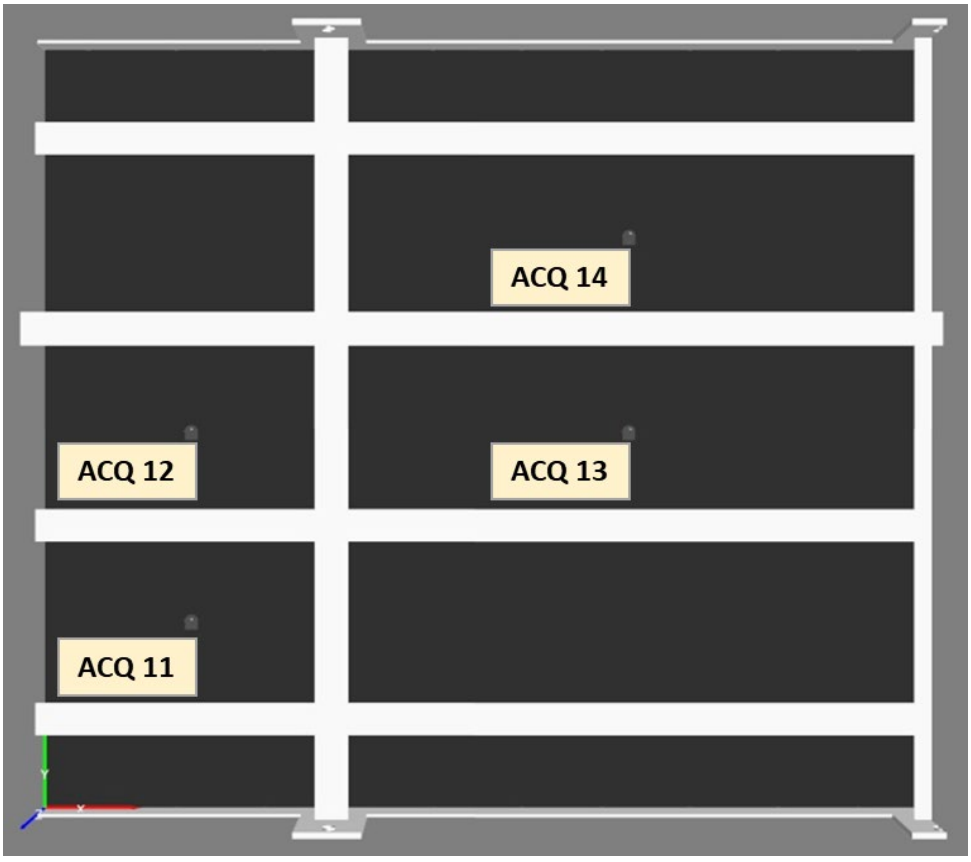

Figure 23. A view (along the z-axis) of the grillage model with the ACQ nodes labeled and the x-y coordinates defined

5.1 Baseline Image Scans

As briefly outlined, the visualization algorithms incorporate hybrid beamforming techniques to provide structural scan images of likely damage locations. The most likely areas of damage are visually indicated. Prior to looking at the structural scan images of specific data cases, it may be helpful to look at baseline data to gain more insight into wave propagation in the structure. In Figure 24, we can see the pulse-echo scan images for the A_0 mode from 60 kHz up to 180 kHz. Typically, the reference baseline dataset is subtracted from the test case under consideration, but these images compare the baseline data set with no subtraction. In a sense, these figures show the attenuation of the excitation signal as it propagates through the grillage. Another way to think about these scans is to consider them a rough estimate of the range of detectability, both for individual nodes and a whole group of nodes. After data collection, node ACQ 11 was found to have intermittent electrical connective to the actuator channel. To avoid confusion, ACQs 12–14 will be utilized for the majority of the results. Pitch-catch data is limited to the path between ACQ 13 and ACQ 14.

There are several interesting conclusions noted in Figure 24. As one may expect, the lower frequencies have lower attenuation, and thus can propagate waves further in the structure from the point of actuation. Additionally, attenuation of the wave energy across the ribs is observed. This effect is a tunable feature in the analysis algorithms and is further described in Figure 25 and Figure 26.

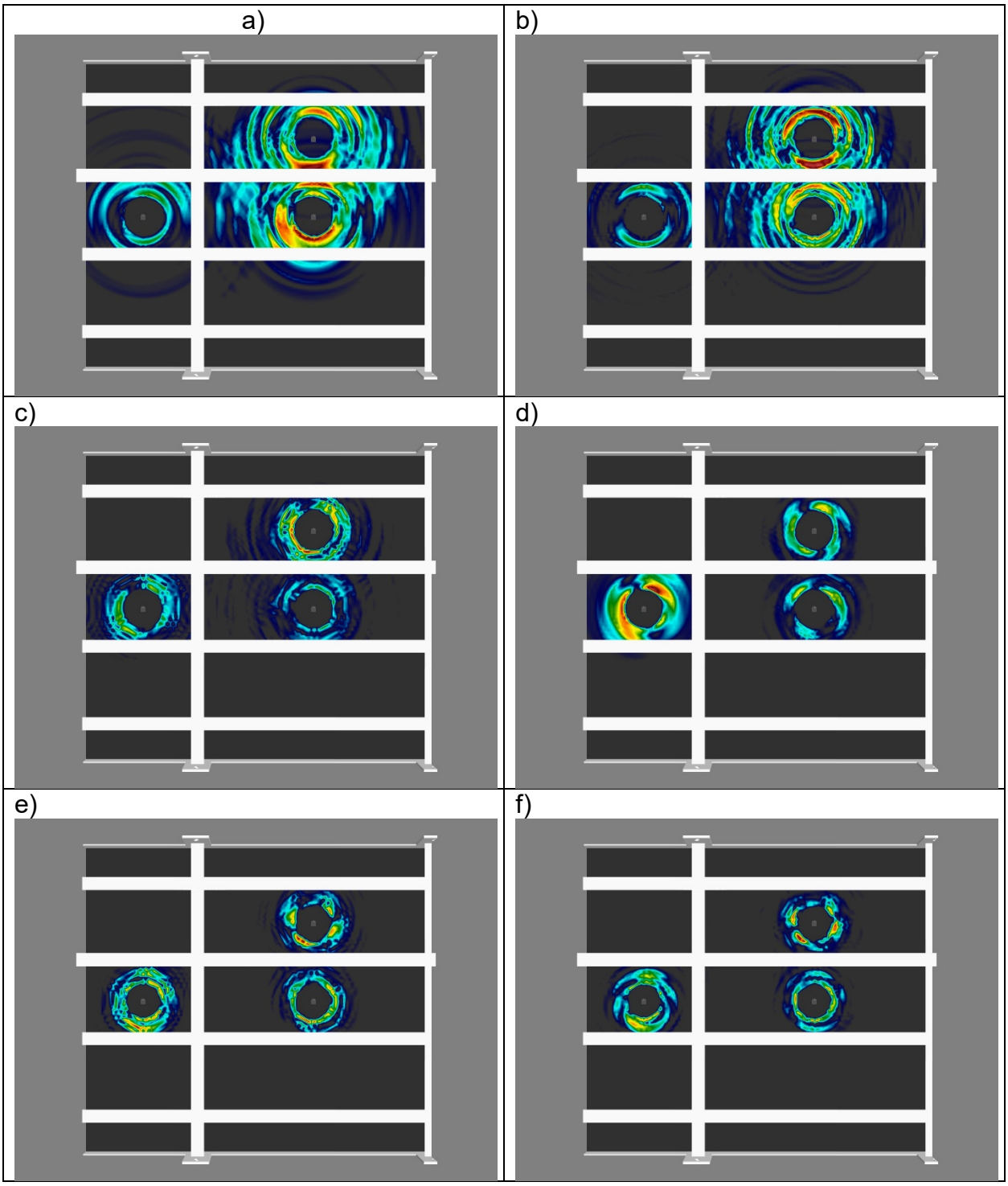

Figure 24. Baseline pulse-echo A_0 image maps for ACQs 12–14 at 60 kHz (a), 80 kHz (b), 100 kHz (c), 120 kHz (d), 160 kHz (e), and 180 kHz (f)

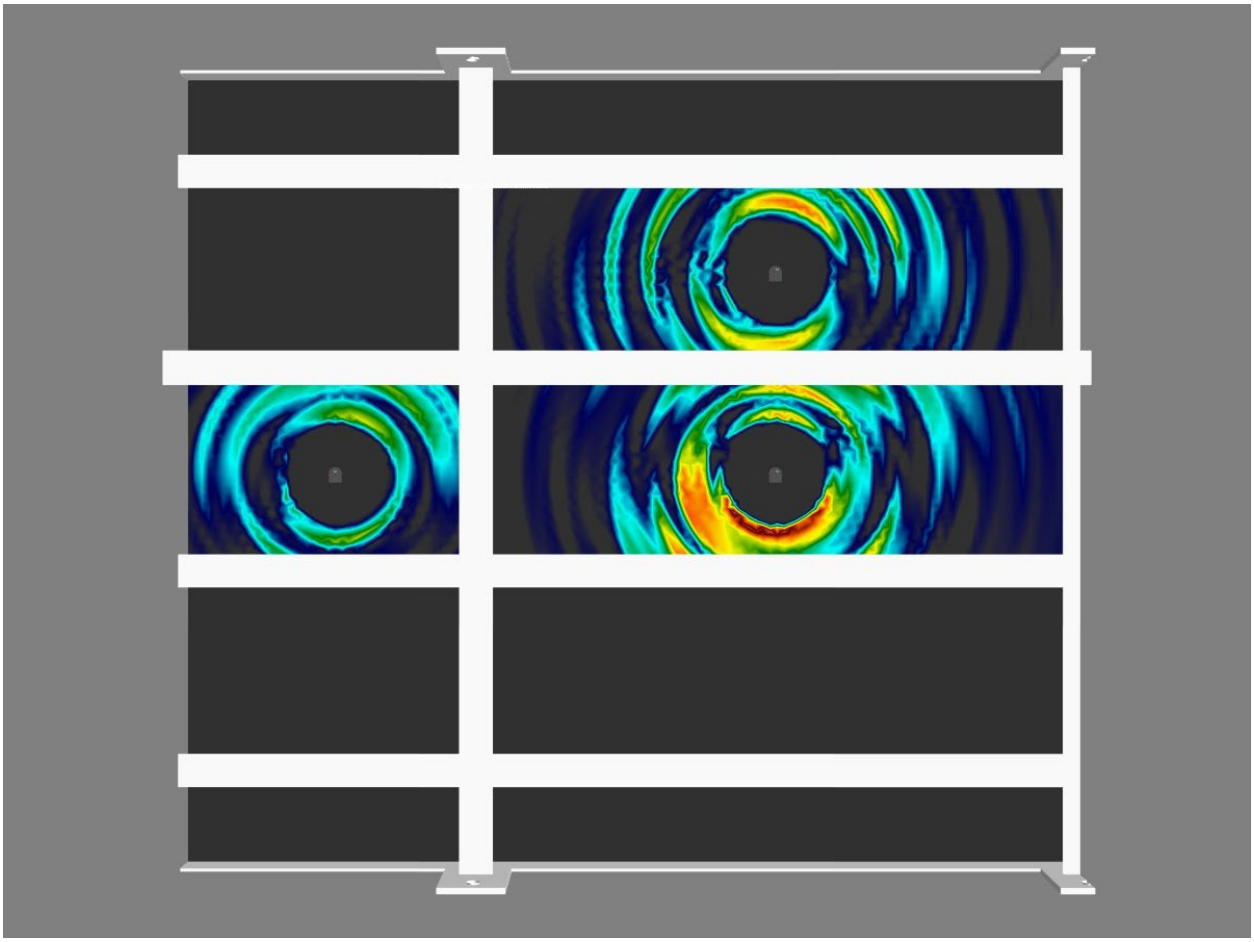

Figure 25. Baseline pulse-echo A_0 image maps for ACQs 12–14 at 60 kHz with a geometry crossing value of 0

Figure 25 and Figure 26 both show the same baseline A_0 image maps for ACQs 12–14 at 60 kHz, with one parametric change in the analysis. The tunable parameter called “geometry crossing scale” allows a user to set signal attenuation when it crosses a physical feature, which are welded stiffeners for this example. In Figure 25, the geometry crossing value is set to 0, assuming that no signal propagates past stiffeners. Conversely, Figure 26 shows the results of a geometry crossing value of 1, which ignores the presence of the welds and stiffeners. Unless otherwise noted, the geometry crossing will be set to 0.5 for the purposes of our analysis. We will assume 50% of the wave propagation energy is attenuated by welds and stiffeners. Propagation of waves across welds in relevant navy materials and structures has been previously investigated (Grisso *et al.*, 2011a and 2011b), so this setting is likely conservative.

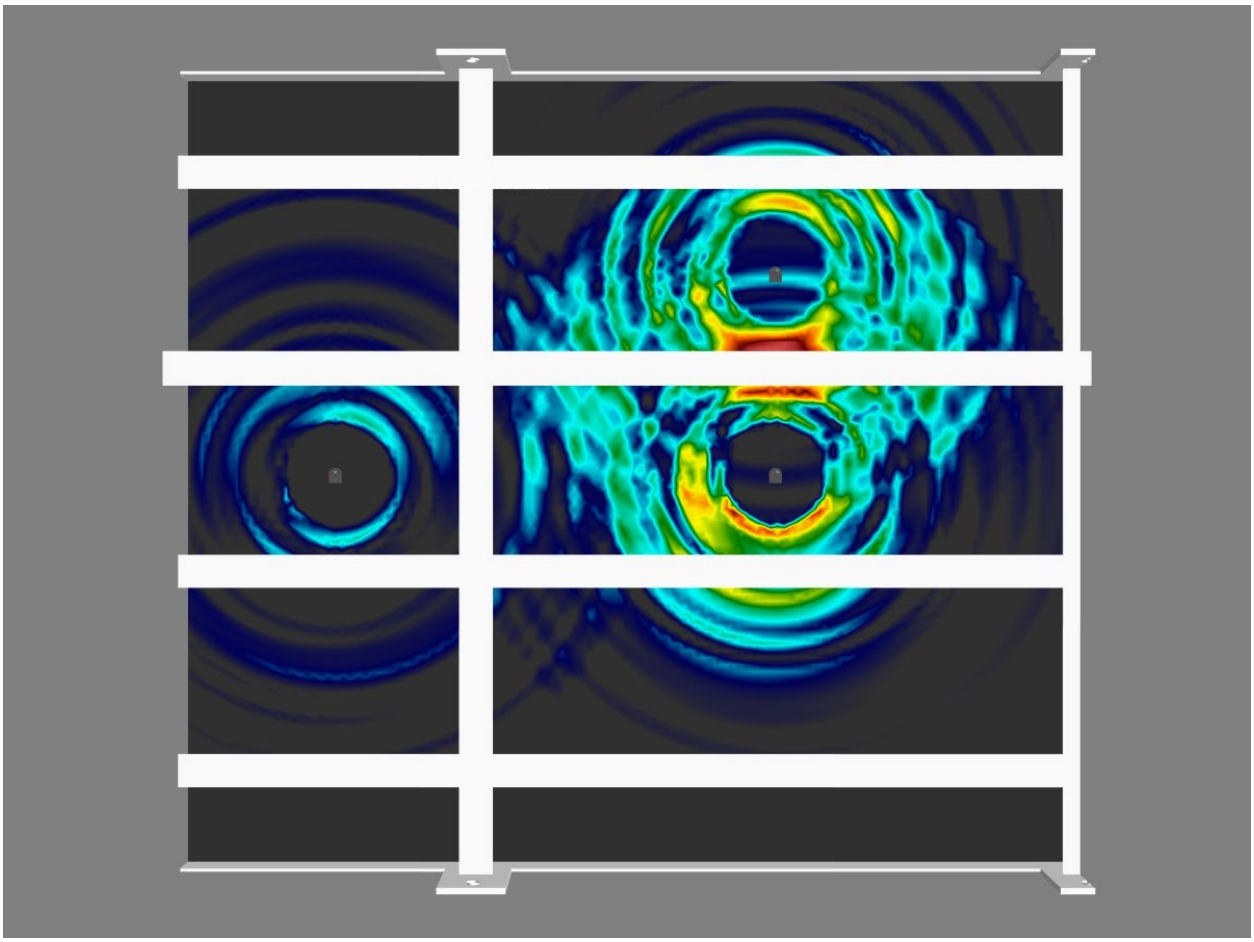

Figure 26. Baseline pulse-echo A_0 image maps for ACQs 12–14 at 60 kHz with a geometry crossing value of 1

Similar to Figure 24, the baseline wave attenuation of the S_0 mode is displayed in Figure 27. The symmetric modes propagate slightly further than the antisymmetric mode at any given frequency, which is expected when considering the dispersion curves (Figure 8). For any excitation frequency, the S_0 wavenumber is smaller, meaning the wavelength is longer. Longer wavelengths should travel greater distances in plate-like structures.

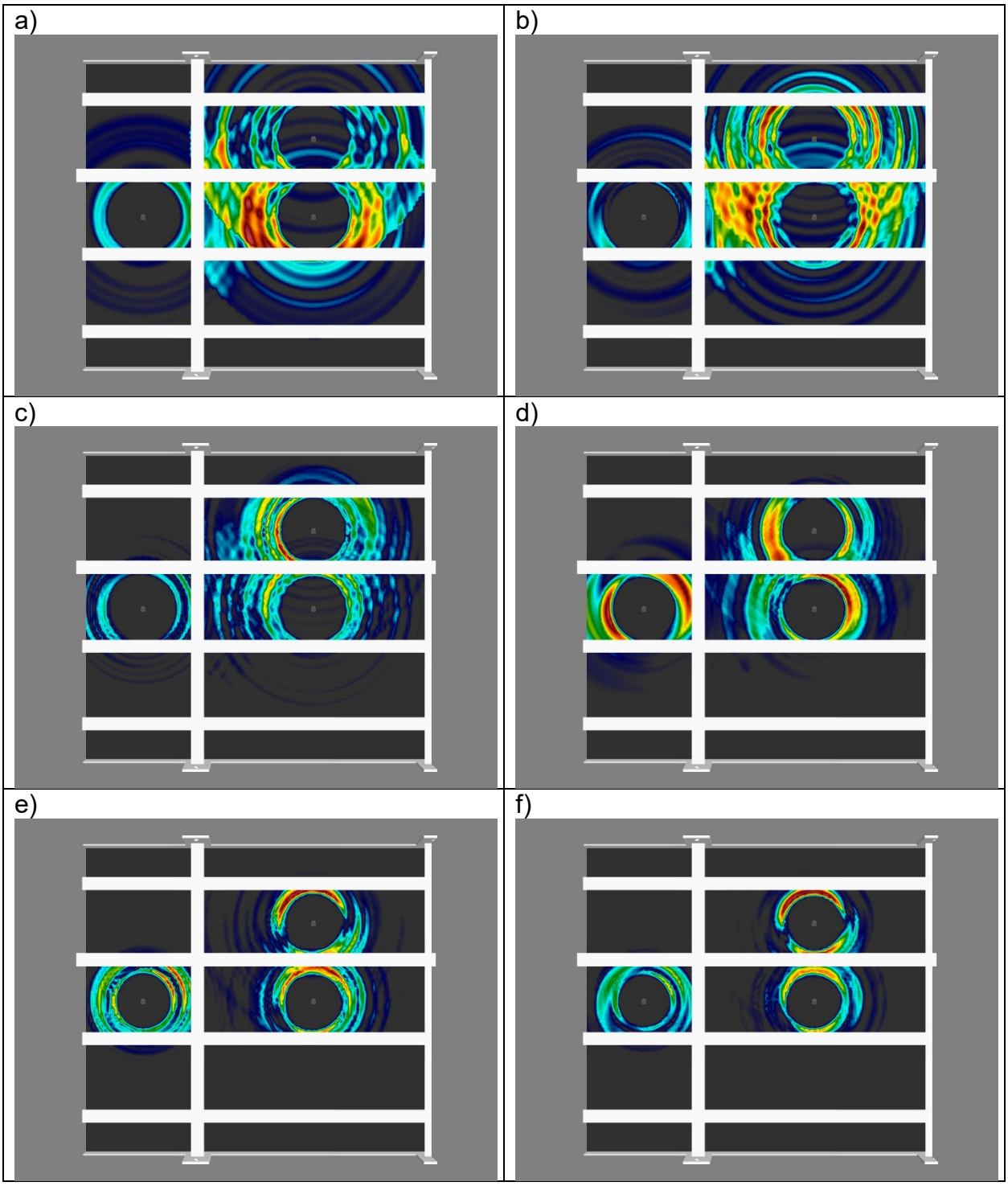

Figure 27. Baseline pulse-echo S_0 image maps for ACQs 12–14 at 60 kHz (a), 80 kHz (b), 100 kHz (c), 120 kHz (d), 160 kHz (e), and 180 kHz (f)

The final set of baseline images to look at are the pitch-catch scans. In Figure 28, we can see 80-kHz A_0-mode image maps with ACQ 13 as the actuator and ACQ 14

as the sensor on the left and with the reverse path on the right. Pitch-catch baseline scans show a slightly larger sensing range than a straight-line path from the actuator to sensor. The sensing capabilities of both pitch-catch and pulse-echo methods will be further demonstrated when analyzing the damage cases.

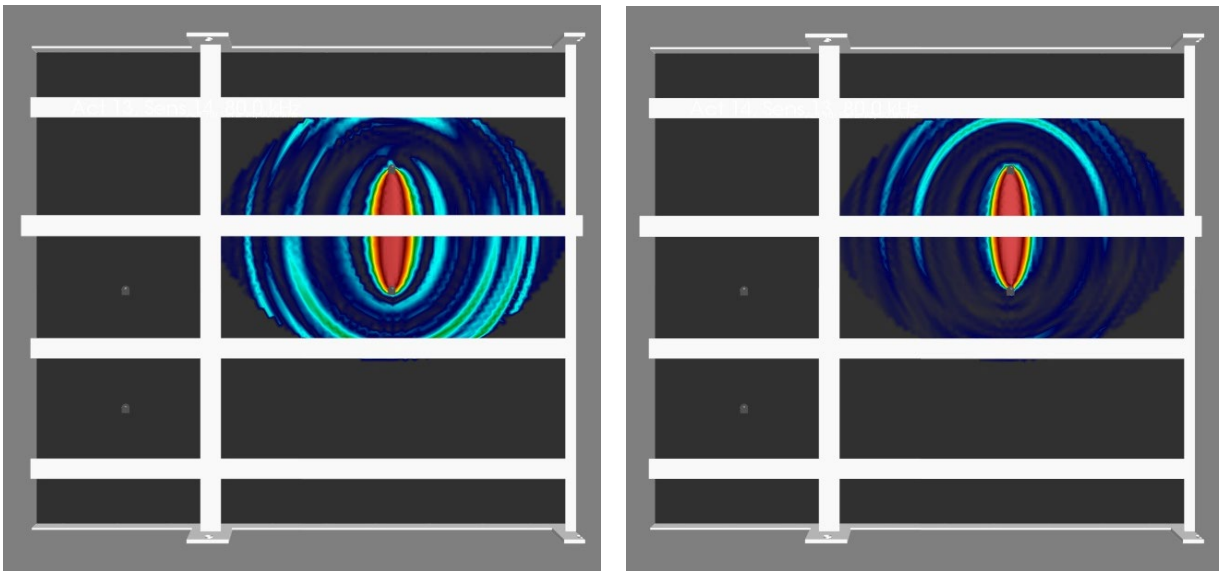

Figure 28. Baseline pitch-catch A_0 image maps for 80 kHz of ACQ 13 excitation (left) and ACQ 14 actuation (right)

5.2 Damage Evaluation

Now that we understand some basic insight into wave propagation of the grillage, we can evaluate each of the damage cases described in Table 1.

5.2.1 Damage 1

As previously mentioned, Damage 1 is a ¼-inch through-hole in the grillage plating. One additional parameter in the processing software, the “Scale Below” feature, will be highlighted before proceeding with the results. Scale below is simply a 0–1 thresholding variable used to define the scale of the image map. With a low threshold value, the range of change over the entire sensing area is visually defined. As the threshold value is raised, only the most likely target areas are highlighted, assisting the user in localizing potential significant changes to the structure. The

underlying data remains the same. To illustrate an example of the thresholding function, different scaling threshold values of the same dataset are visible in Figure 29.

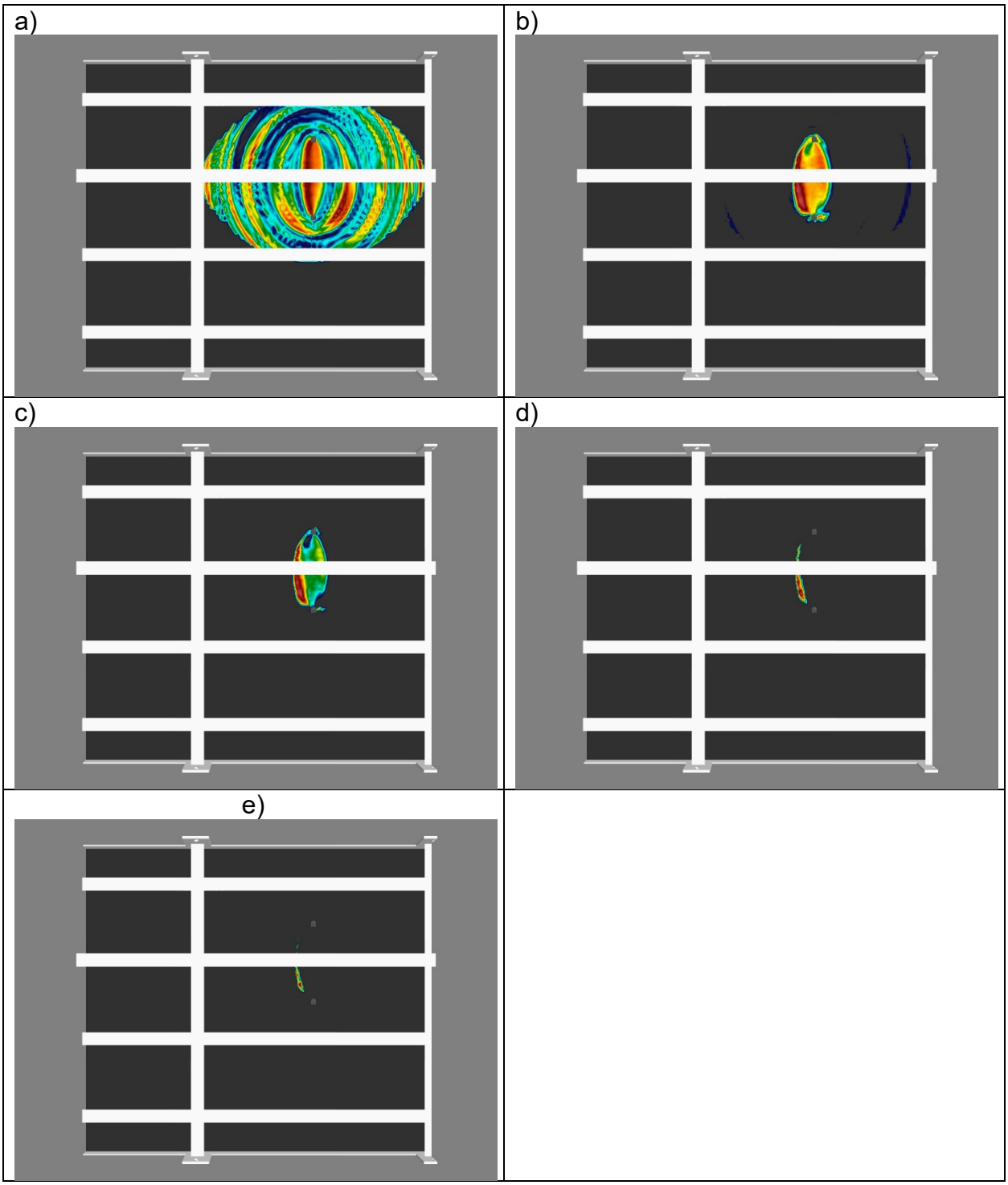

Figure 29. Pitch-catch A_0 results between ACQ 13 and ACQ 14 with scaling threshold values of 0.1 (a), 0.5 (b), 0.7 (c), 0.9 (d), and 0.95 (e)

As Figure 29 reveals, at low threshold values, the significant potential damage targets can be difficult to pick out of the entire field of change. Lamb waves are dispersive, so the spatial wave field may be significantly altered due to new reflections, wave mode conversions, different wave interactions, etc. The threshold tool provides visually apparent representations of the most likely wave scattering sources. In future plots, the threshold will be adjusted for simple visual comparisons of estimated damage locations versus actual locations.

Next, the effect of different excitation frequencies on damage detectability will be presented. Figure 30 shows select frequencies from 60 kHz to 180 kHz of the A_0 pitch-catch data between ACQ 13 and ACQ 14. Knowing the true location of the damage (Figure 14, Table 1), we can easily infer that lower excitation frequencies do not provide accurate localization insight. Around 100 kHz, the results start to indicate the true hole location. By 140 kHz, the estimated damage location is readily apparent. These results are not unexpected based upon prior Lamb wave damage detection research.

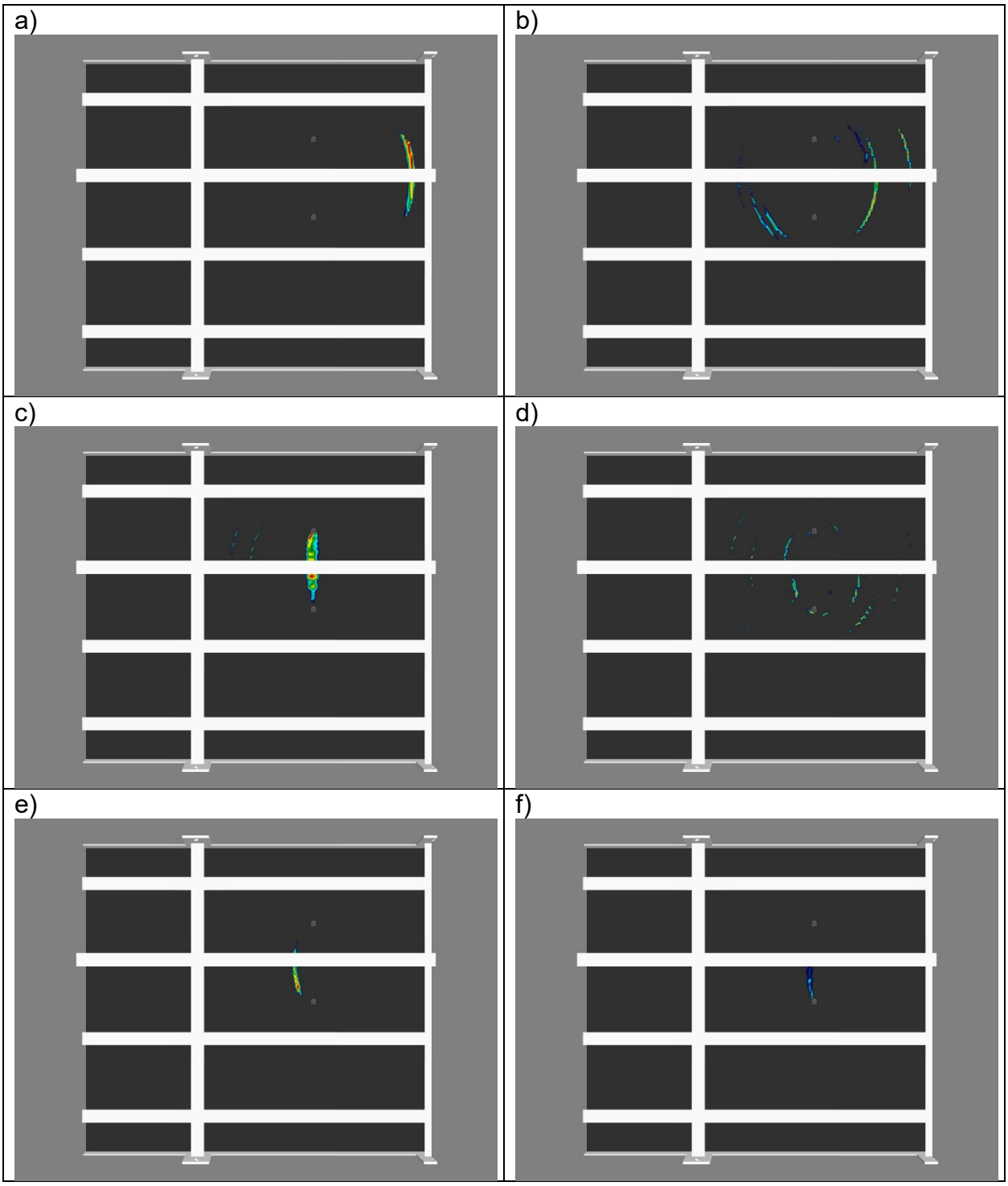

Figure 30. Pitch-catch A_0 results between ACQ 13 and ACQ 14 with narrowband frequency reconstructions of 60 kHz (a), 80 kHz (b), 100 kHz (c), 120 kHz (d), 140 kHz (e), and 80 kHz (f)

Continuing the analysis of pitch-catch data for Damage 1, we can look more closely at one of the frequencies which appears sensitive to the presence of damage.

Figure 31 shows the image map for 160-kHz narrowband A_0 pitch-catch results between ACQ 13 and ACQ 14. Adjusting the threshold, we see that the analysis reveals that the experimentally determined damage source appears accurate. To verify this, we can map the actual damage location onto the image map. The bright green square in Figure 32 identifies the physical location of the through-hole on the structure. The predicted damage source matches the actual location closely, and the square is somewhat difficult to distinguish.

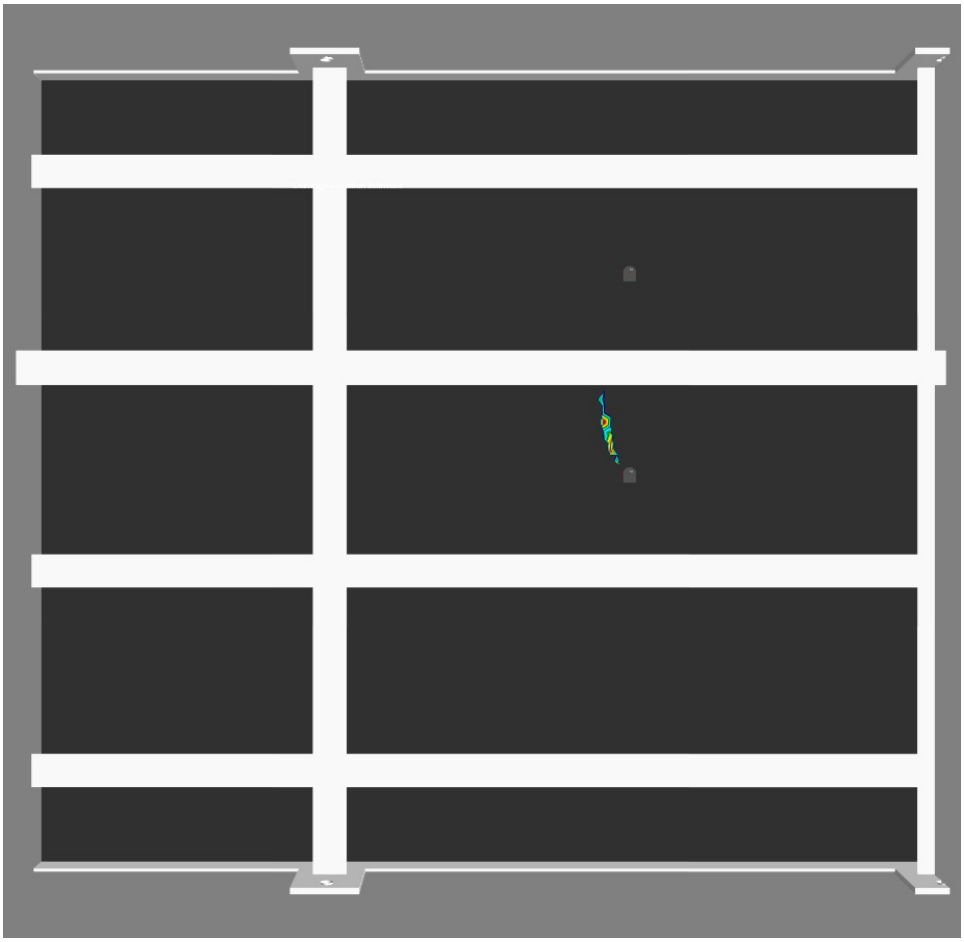

Figure 31. Experimentally determined source of damage shown for 160-kHz A_0 pitch-catch results between ACQ 13 and ACQ 14 for Damage 1

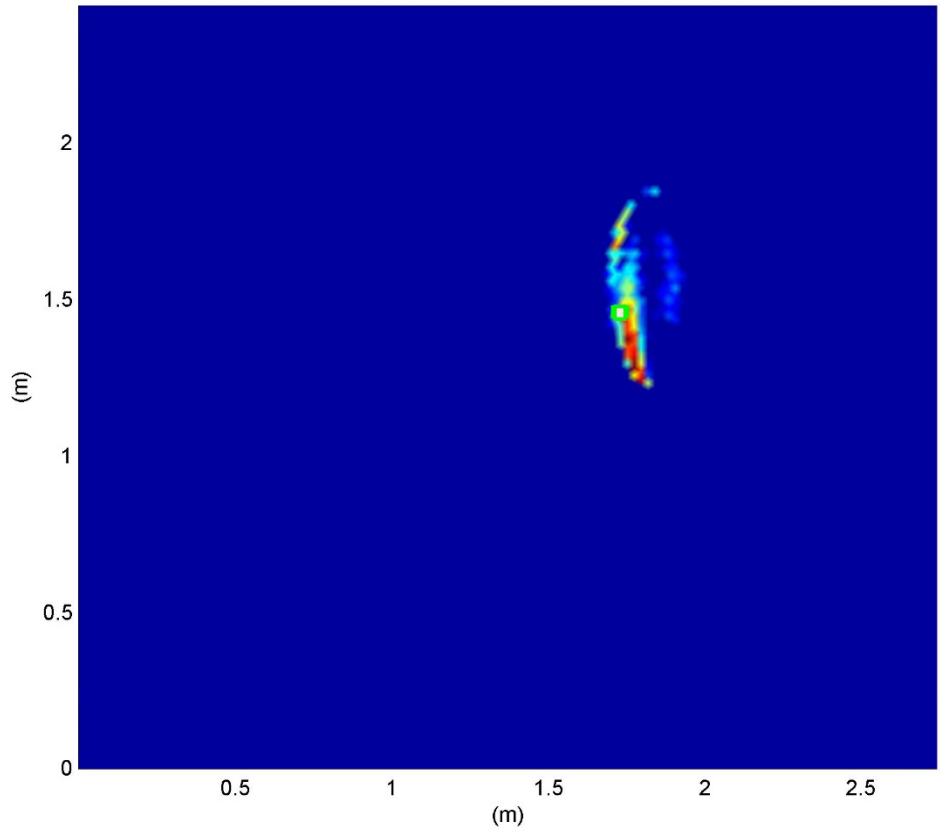

Figure 32. The actual damage location (bright green square) and experimentally determined source of damage shown for 160-kHz A_0 pitch-catch results between ACQ 13 and ACQ 14 for Damage 1

Next, we will look at the pulse-echo results. Phase-coherent beamforming results combining the data from ACQ 13 and ACQ 14 are used to detect the hole. Figure 33 shows the image map generated using the 150-kHz S_0 mode, while Figure 34 overlays the actual damage location. Figure 35 contains similar results for the 160-kHz S_0-mode narrowband reconstruction.

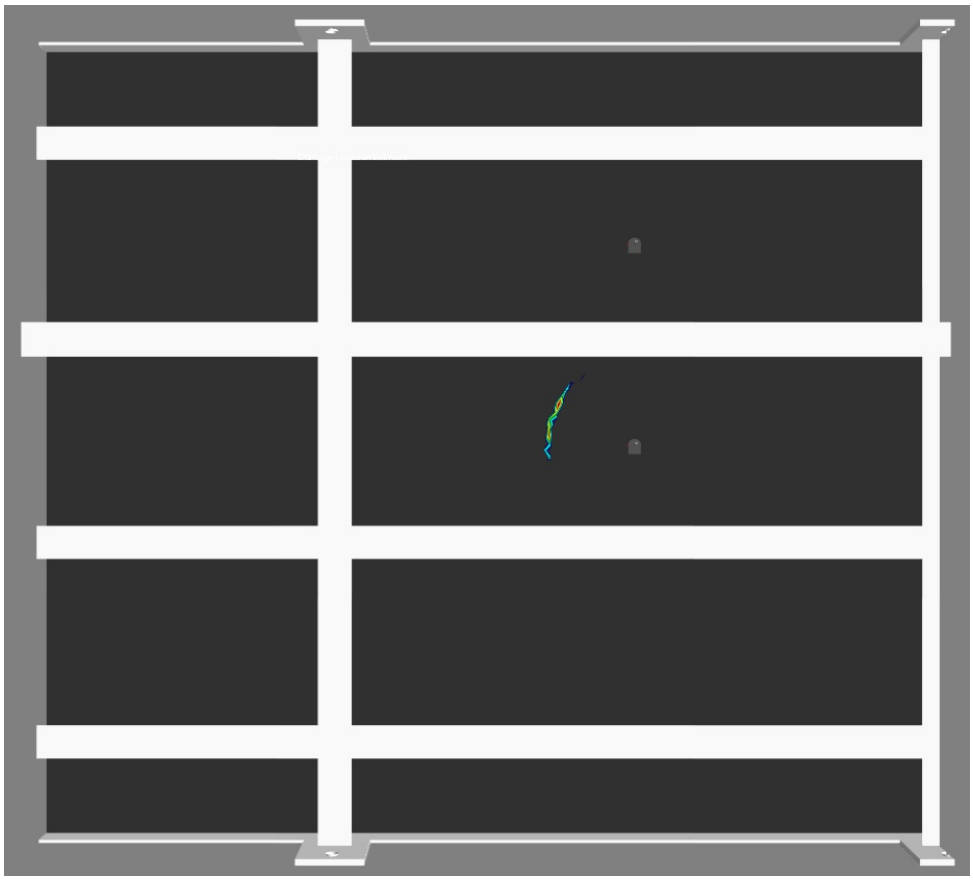

Figure 33. ACQ 13 and ACQ 14 150-kHz S_0 pulse-echo image maps

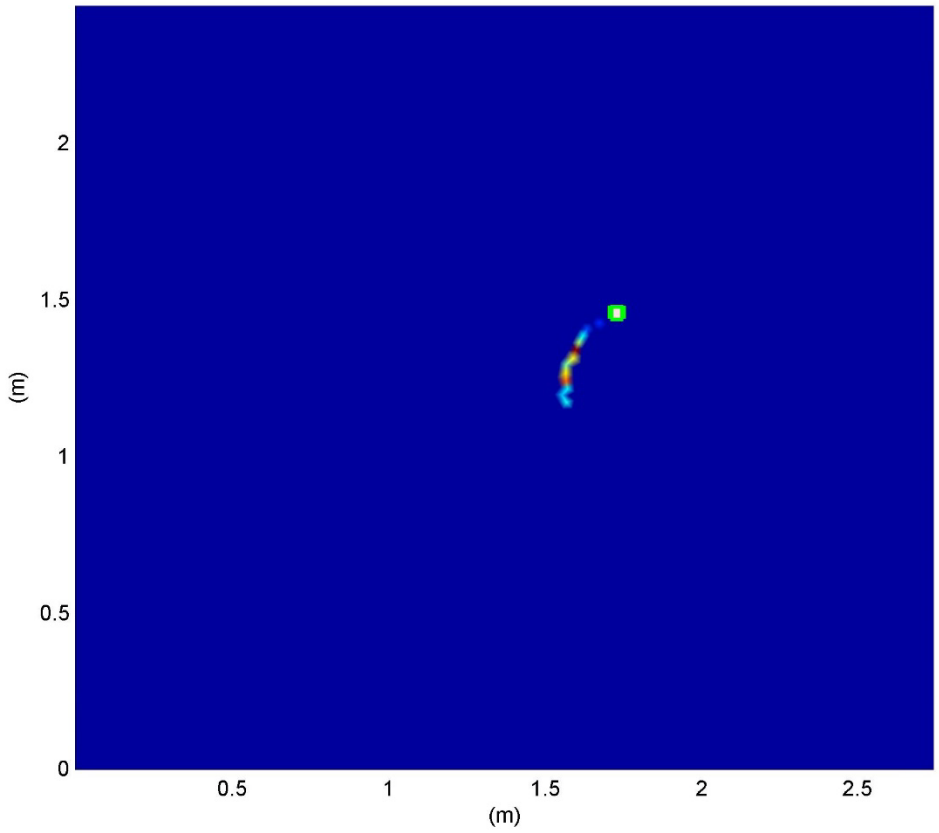

Figure 34. The actual damage location (bright green square) and experimentally determined source of damage shown for 150-kHz S_0 pulse-echo image maps from ACQ 13 and ACQ 14

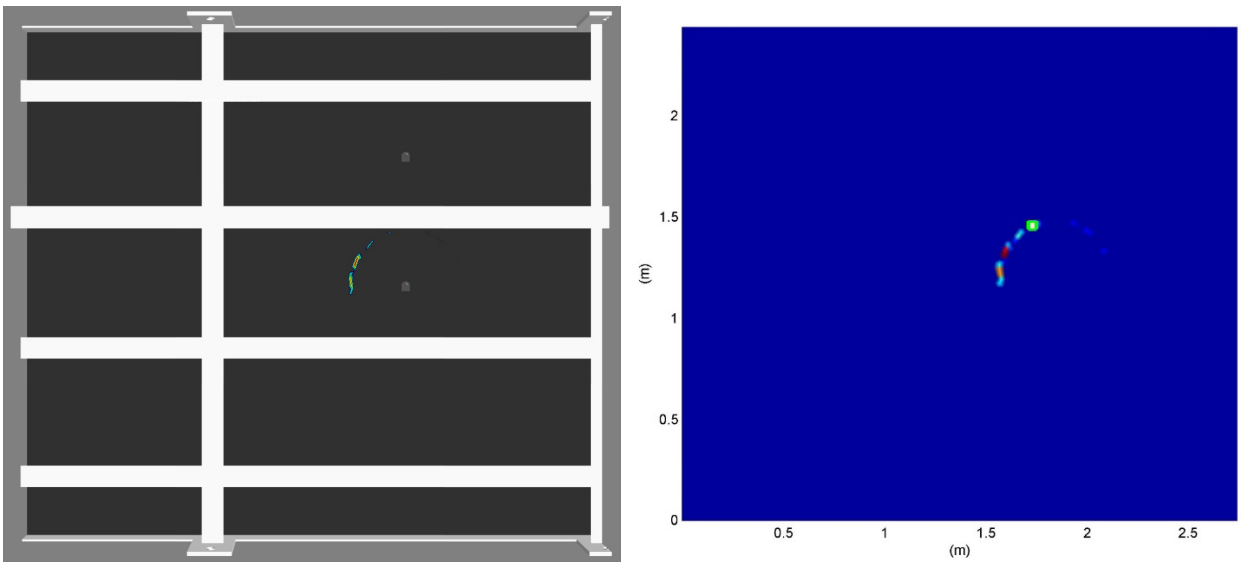

Figure 35. ACQ 13 and ACQ 14 160-kHz S_0 pulse-echo image maps (left) and the actual damage location (bright green square) with experimental results (right)

The pulse-echo technique determines the radial distance of the damage quite effectively. However, with only one node between longitudinal stiffeners, accurate triangulation of the angular location of the damage suffers. Still, the results are very promising for detecting a small source of damage on a large grillage structure.

The interaction between the S_0 mode and a circular inclusion in a plate has been extensively studied, numerically, analytically, and experimentally (Diligent *et al.,* 2002; Fromme and Sayir, 2002; Moreau *et al.,* 2011; McKeon and Hinders, 1999). In one such study, Diligent *et al.* (2002) measured reflections from circular defects analytically, numerically (Finite Element simulation), and experimentally and noted very good results when the hole diameters were in the range of one to three wavelengths of the excitation center frequency wavelength. As a reference, the S_0-mode wavelength in our material is approximately 3.3 inches at 60 kHz, scaling down to 1.1 inches at 180 kHz. For a ¼-inch hole, the wavelength-to-hole diameter ratios fall between 0.07 to 0.27, orders of magnitude smaller than the mentioned study. Ideally, for damage detection, it is helpful to have a wavelength at least half the linear dimension of the damage length to ensure interaction of the waves with the defect. Longer wavelengths may be unaffected by small amounts of damage. Thus, the result indicating only higher frequencies are sensitive to the hole damage is typical based on previous research.

A second consideration for damage detection sensitivity is the electro-mechanical coupling between the piezoelectric actuator and the structure. Giurgiutiu (2014) extensively details, analytically and experimentally, the interaction between circular piezoelectric transducers bonded to a host structure (thin or thick plates). Piezoelectric transducers are strain-coupled actuators and sensors when bonded to a structure. At certain frequencies, considering the geometry and properties of both the transducer and host plate, a piezo can more efficiently generate ultrasonic waves. In other words, for a constant applied voltage to the transducer, the strain generated is variable with respect to frequency. This characteristic can be utilized to tune excitation frequencies for both efficient structural actuation and sensing.

Using freely available software (Waveform Revealer 3), the interaction between the bonded structural sonar actuator and the grillage plating can be determined. Figure 36 shows the theoretical normalized strain amplitudes versus frequency for the S_0 and

A_0 modes coupled with a 0.35-inch-diameter circular piezoelectric actuator. The input signal of a 160-kHz narrowband excitation is also shown. For the A_0 mode, we see the maximum strain induced on the plate from the actuator (under 400 kHz) is around 100 kHz. Similarly, the optimal tuning value for S_0 is around 200 kHz.

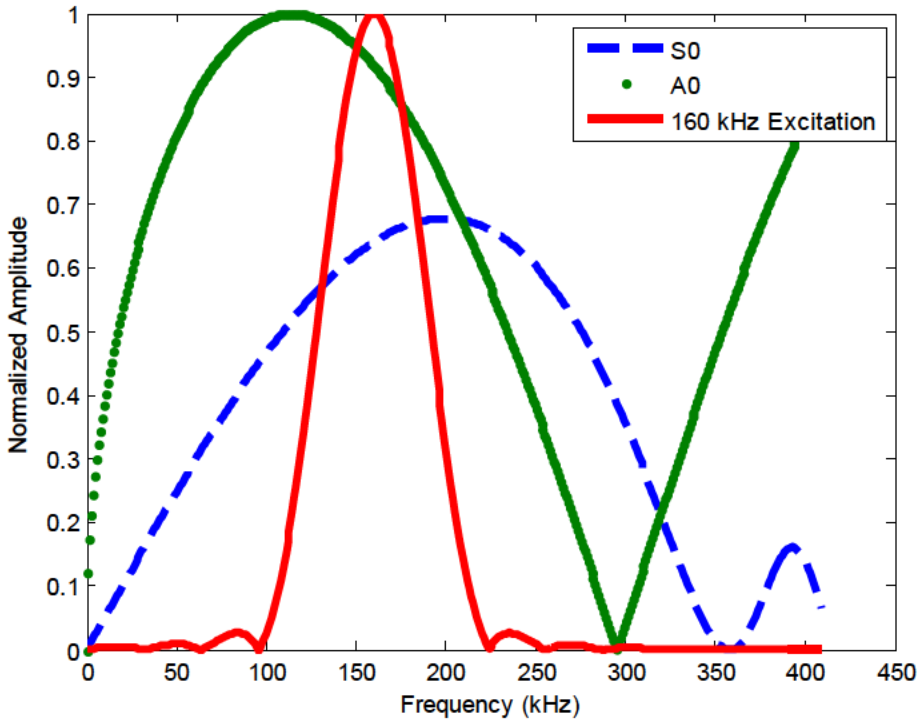

Figure 36. Theoretical normalized strain amplitudes plotted with a 160-kHz narrowband excitation for a 0.35-inch diameter circular piezoelectric actuator bonded to a ¼-inch A36 steel plate

The net insight from previous research into through-hole reflectivity and plate Lamb wave tuning, provides an awareness that, due to the wavelengths of Lamb waves in our material, we would expect only higher frequencies to be sensitive to the presence of small amounts of damage. Also, as the frequency of S_0 actuation increases, we will theoretically move into a region of more efficient plate excitation. Both results validate our experimental results showing optimal detection of Damage 1 above 140 kHz.

5.2.2 Damage 2

The second damage condition is a simulated crack in a transverse stiffener weld toe. A picture of Damage 2 and the remaining damage cases are located in Appendix

B. Looking at the Lamb wave attenuation scans (Figure 24 and Figure 27), it is expected this damage case will be on the fringes of the detectable region for the current ACQ-node configuration. The damage is well outside of the pitch-catch path, so we will briefly look at pulse-echo results.

In Figure 37, we can see the antisymmetric, pulse-echo image maps for 60 kHz. Figure 38 and Figure 39 show the actual damage location (at the far right) and image maps for 60 kHz and 65 kHz, respectively. As the results show, there is no clear indication of the damage. In Figure 39, one could make an argument that the image maps reveal wave propagation changes near the damage, but they are not the highest amplitude deviations. With the limitations of sensing range of higher frequency modes combined with the lack of sensitivity to damage of lower frequencies, these results are somewhat expected. Overall, the results are inconclusive and heavily trend toward unsuccessful detection of this damage event.

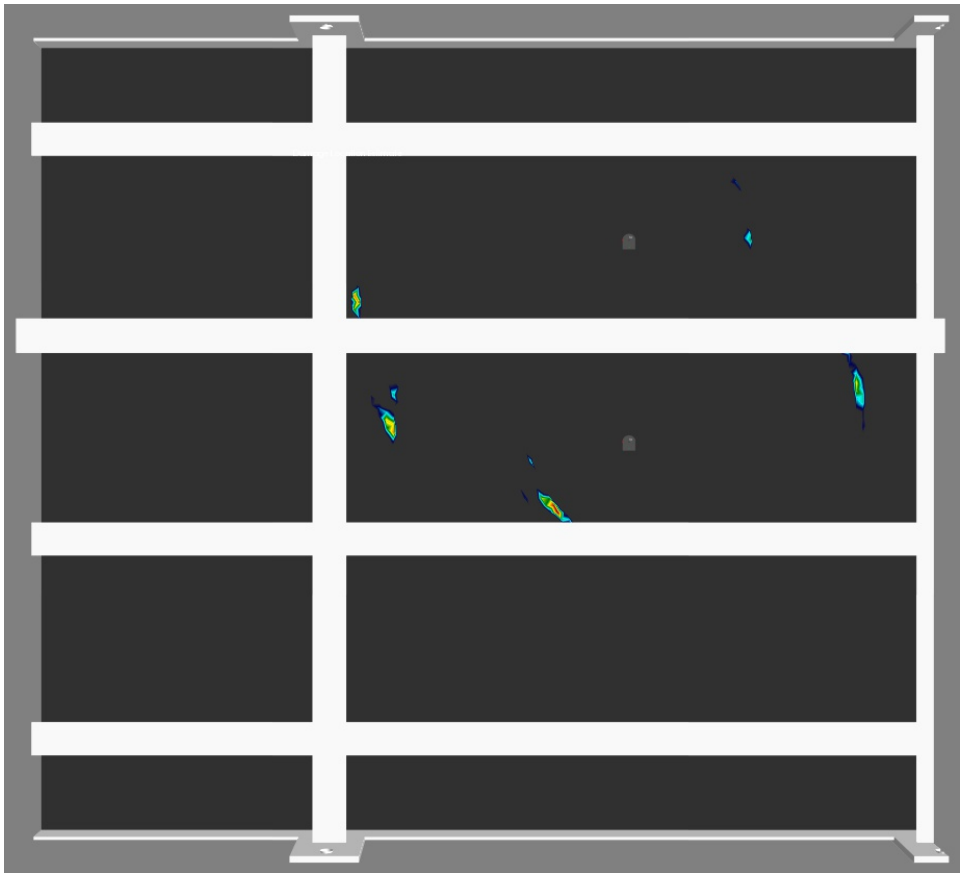

Figure 37. ACQ 13 and ACQ 14 60-kHz A_0 pulse-echo image maps for Damage 2

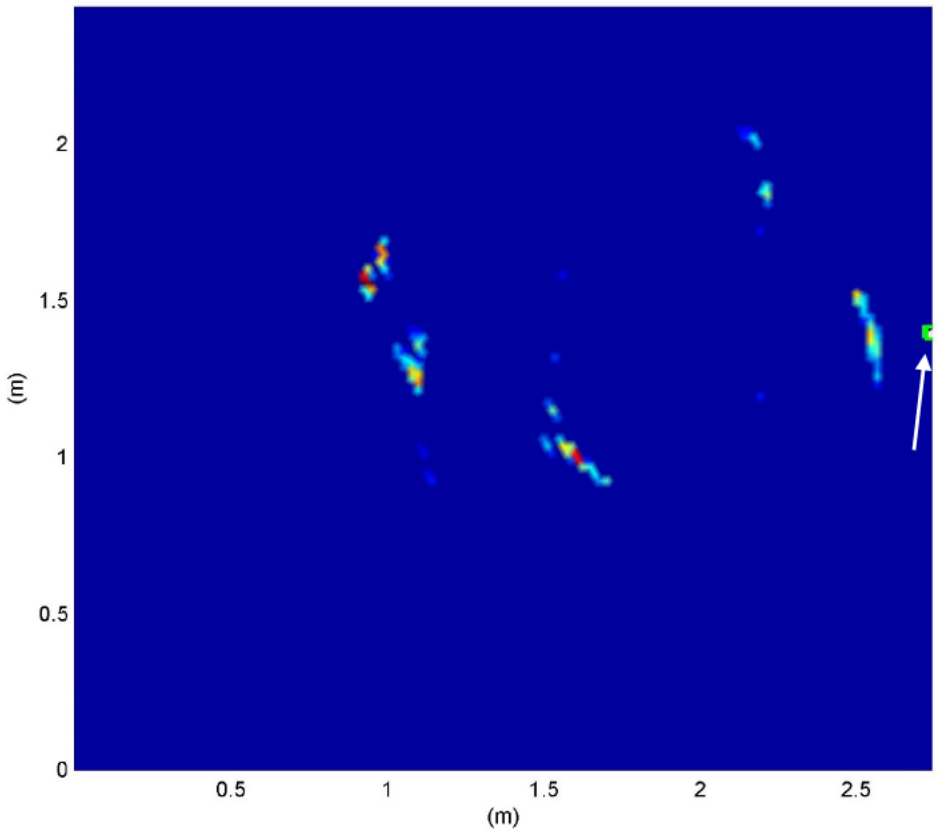

Figure 38. The actual damage location (bright green square) and experimentally determined source of damage shown for 60-kHz A_0 pulse-echo image maps from ACQ 13 and ACQ 14

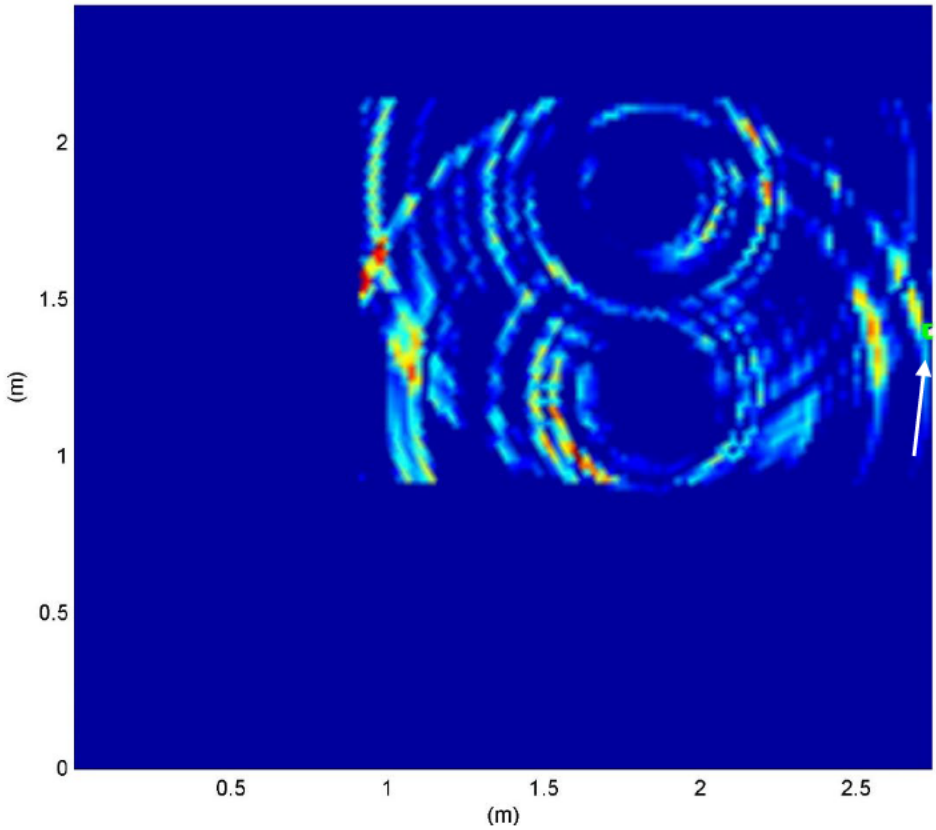

Figure 39. The actual damage location (bright green square) and experimentally determined source of damage shown for 65-kHz A_0 pulse-echo image maps from ACQ 13 and ACQ 14

5.2.3 Damage 3

As shown in Figure 15, Damage 3 is a simulated weld toe crack along a longitudinal stiffener located between ACQ 13 and ACQ 14. Both pitch-catch and pulse-echo detection should be able to detect this damage. Figure 40 shows the 60-kHz A_0 pulse-echo image maps from ACQ 13 and ACQ 14 for Damage 3, while Figure 41 provides the true damage location.

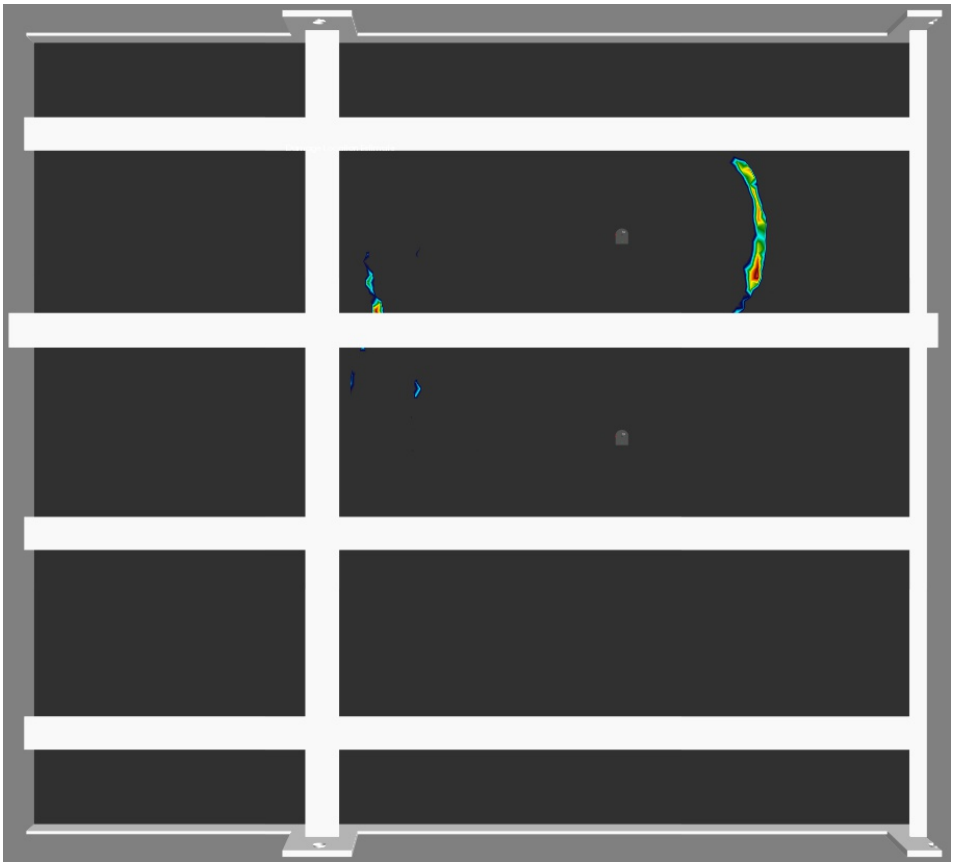

Figure 40. ACQ 13 and ACQ 14 60-kHz A_0 pulse-echo image maps for Damage 3

Much like the pulse-echo results from Damage 1 (Figure 35), the radial component of the damage location is accurate. One more ACQ node may dramatically enhance damage triangulation to narrow the target location. When trying to cover a significant spatial area with limited sensors, the redundancy and location accuracy comes at a cost of less structure coverage. The pitch-catch results shown in Figure 42 and Figure 43 are indicative of a stiffness change along the weld between nodes ACQ 13 and ACQ 14.

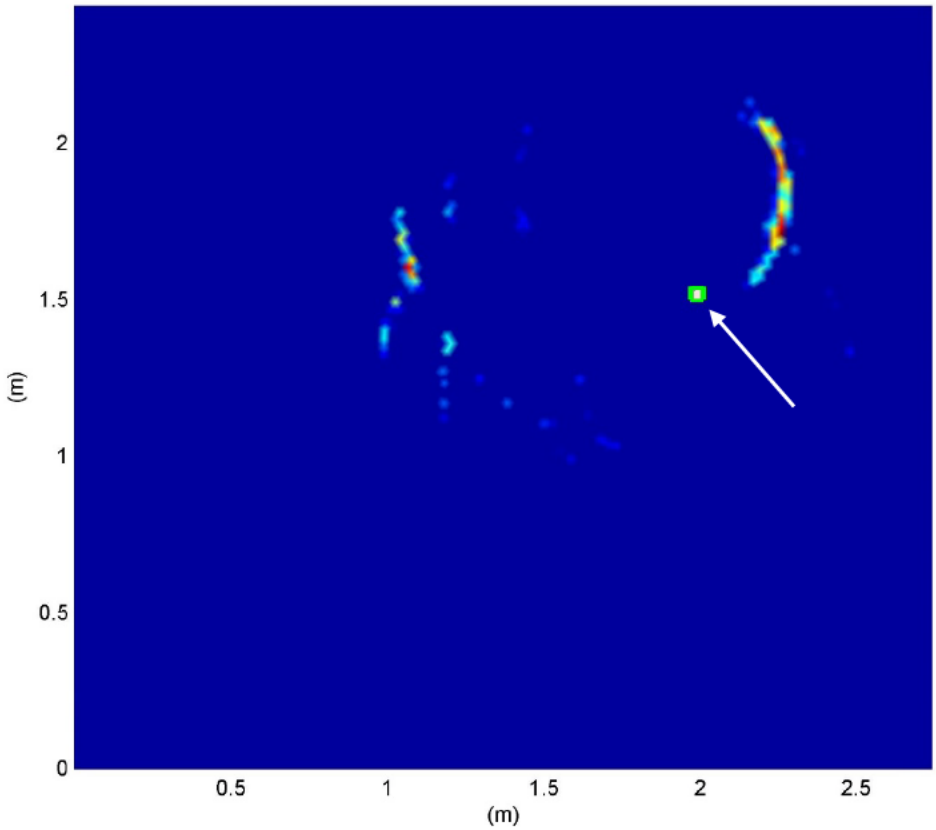

Figure 41. The actual damage location (bright green square) and experimentally determined source of damage shown for 60-kHz A_0 pulse-echo image maps from ACQ 13 and ACQ 14

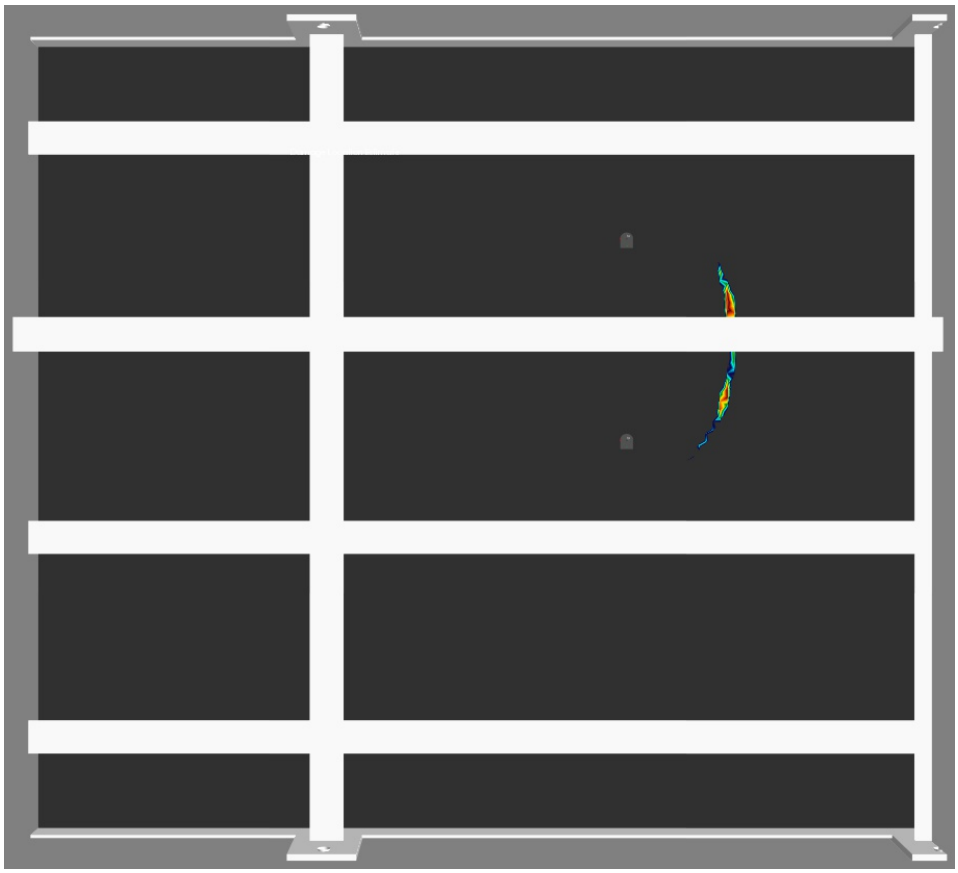

Figure 42. ACQ 13 and ACQ 14 60-kHz S_0 pitch-catch image maps for Damage 3

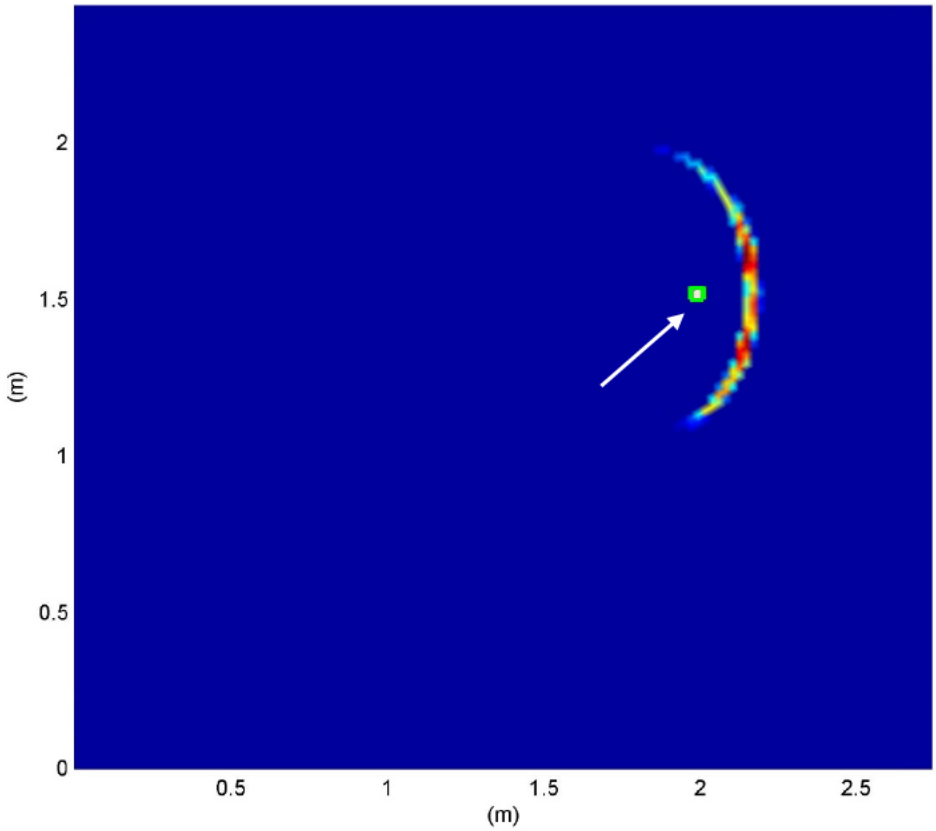

Figure 43. The actual damage location (bright green square) and experimentally determined source of damage shown for 60-kHz S_0 pitch-catch image maps between ACQ 13 and ACQ 14

5.2.4 Damage 4

Damage 4 is a simulated surface crack in the baseplate (Appendix B). The crack is nearest to ACQ 14, and a single node should be capable of discovering its presence. In Figure 44, we see the S_0-mode pulse-echo image map of ACQ 14 for Damage 4 at 50 kHz. As seen previously, the range of the damage relative to the node is accurately identified. Figure 45 reveals the actual crack location, which is near the point indicated as the most likely scattering target.

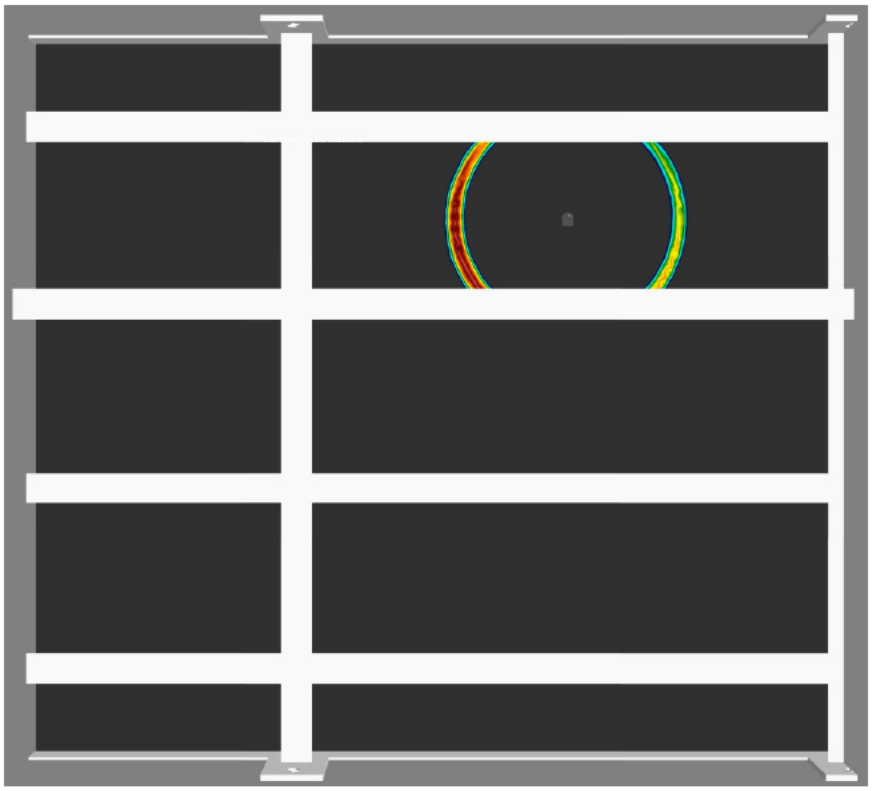

Figure 44. ACQ 14 50-kHz S_0 pulse-echo image map for Damage 4

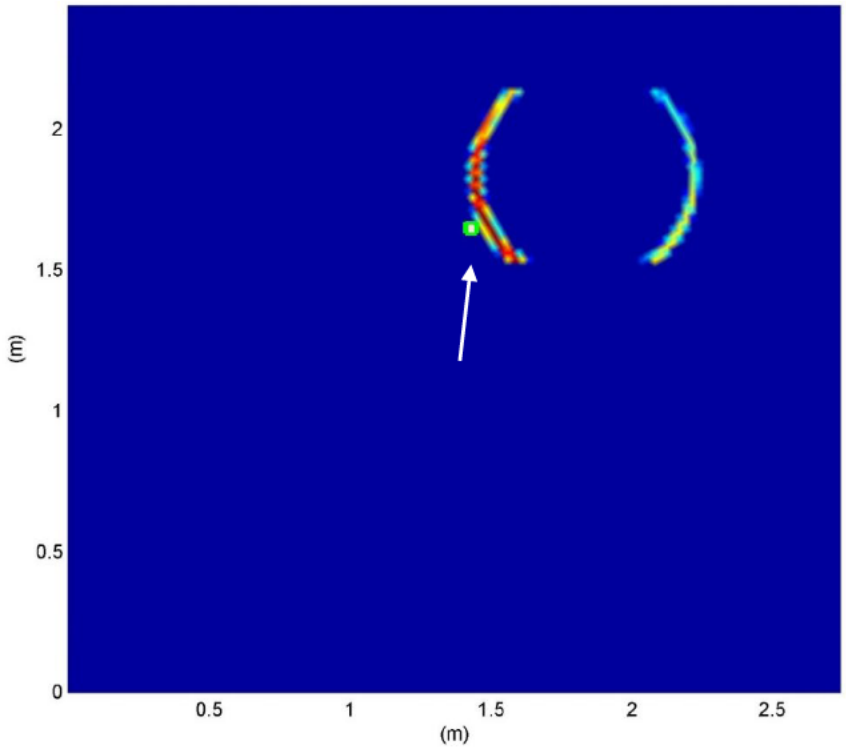

Figure 45. The actual damage location (bright green square) and experimentally determined source of damage shown for a 50-kHz S_0 pulse-echo image map of ACQ 14 for Damage 4

5.2.5 Damage 5

Similar to Damage 2, the fifth damage condition is a simulated crack in a transverse stiffener weld toe. As we observed analyzing the results of Damage 2, we expect only low frequencies to have any sensitivity to the damage. Given the physical limitation of the current setup, pulse-echo will also be the only technique potentially capable of detecting Damage 5. Figure 46 shows the 70-kHz A_0 pulse-echo image map of ACQ 14. Low (Figure 47) and high (Figure 48) threshold image maps show the true location of the damage. The results indicate that ACQ 14 may be sensitive to the damage. The largest noted changes are in the same radial direction as the real crack. The lower frequencies tend to show the same result, with the most likely source of damage shown indicated as toward the location of damage. Figure 49 reveals a similar result for an antisymmetric mode. As with Damage 2, successful damage detection is inconclusive without further studies into the sensitivity of similar damage scenarios.

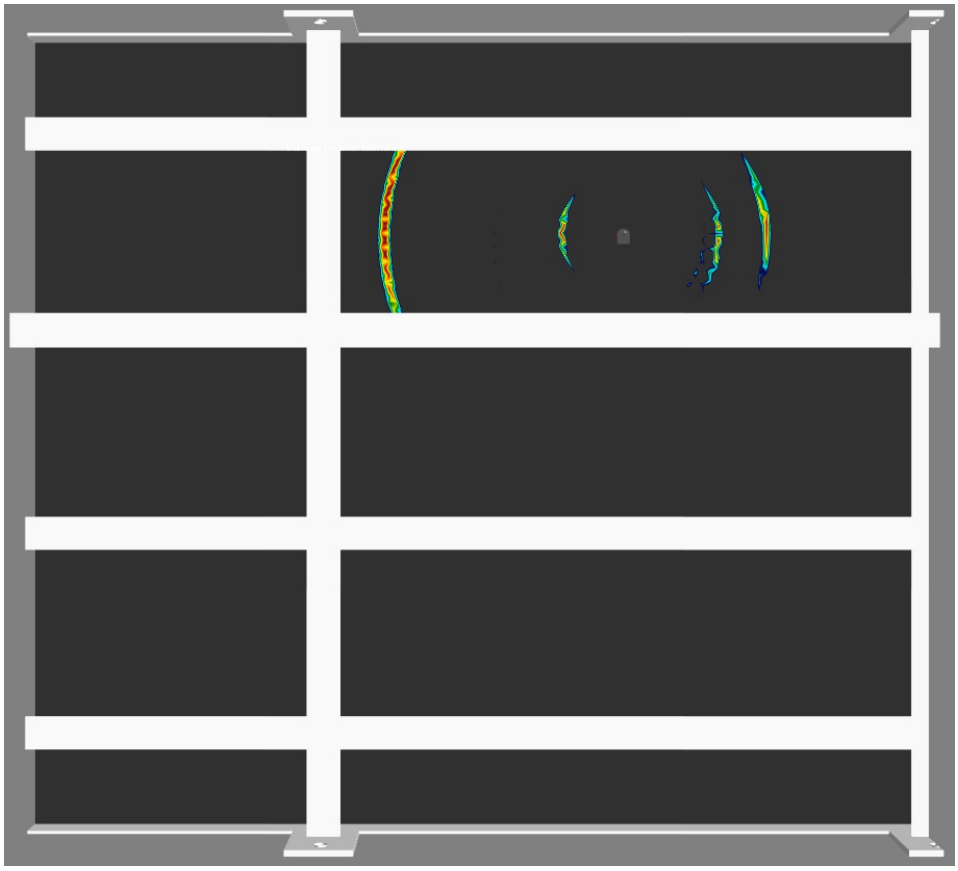

Figure 46. ACQ 14 70-kHz A_0 pulse-echo image map for Damage 5

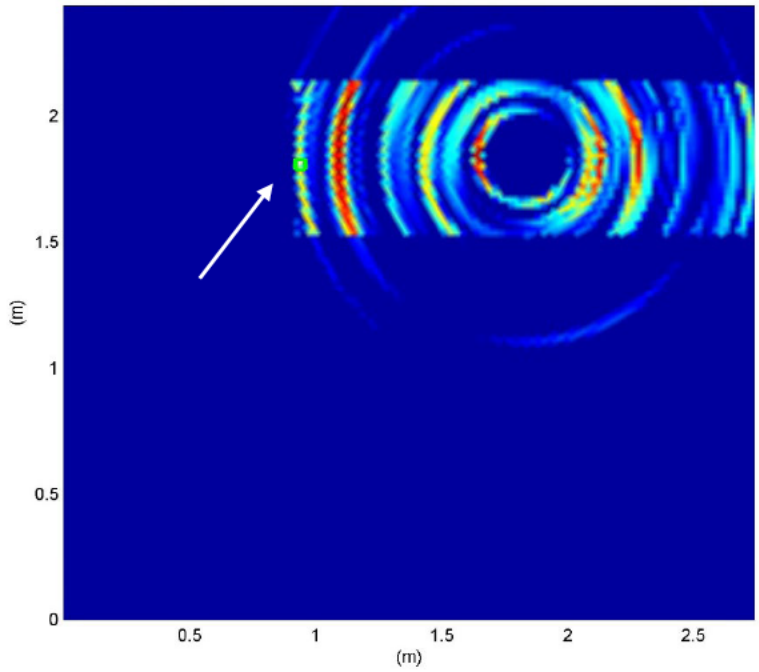

Figure 47. The actual damage location (bright green square) and experimentally determined source of damage shown for a 70-kHz A_0 pulse-echo image map (at a low threshold) of ACQ 14 for Damage 5

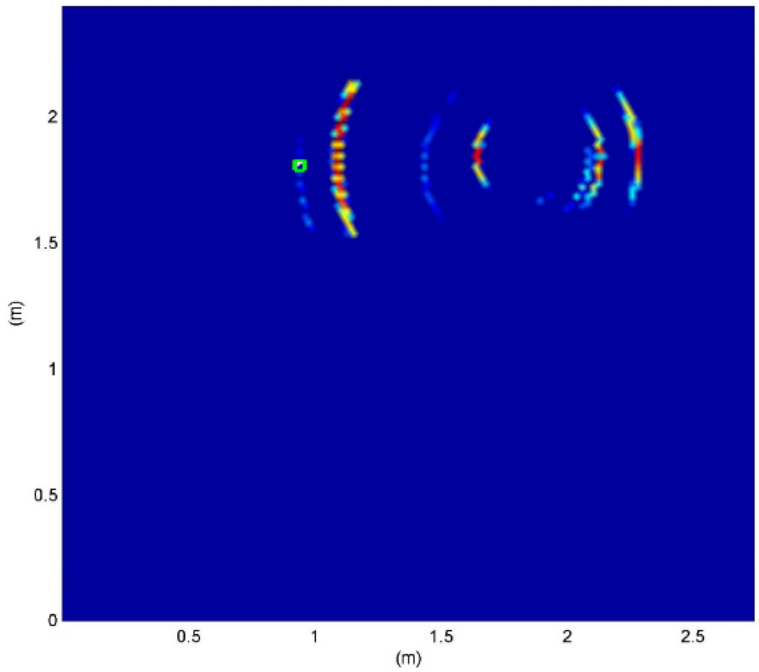

Figure 48. The actual damage location (bright green square) and experimentally determined source of damage shown for a 70-kHz A_0 pulse-echo image map (at a high threshold) of ACQ 14 for Damage 5

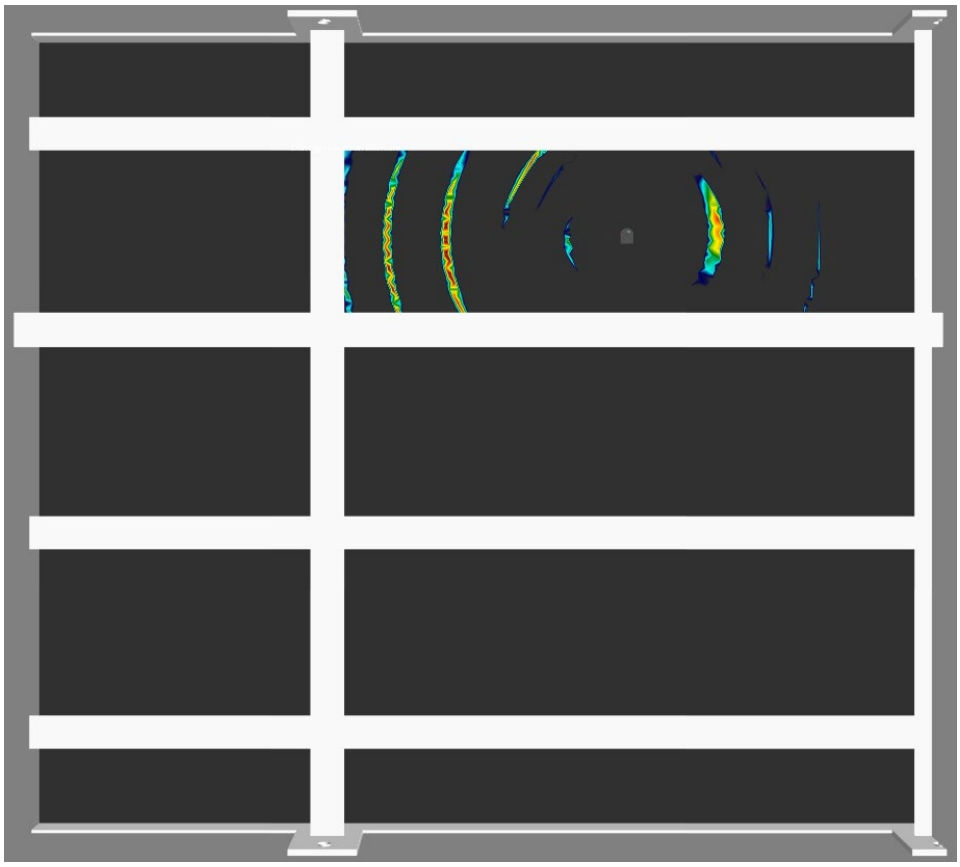

Figure 49. ACQ 14 65-kHz A_0 pulse-echo image map for Damage 5

5.2.6 Damage 6

Similar to Damage 4, Damage 6 is a simulated baseplate surface crack. The damage was introduced with a close enough proximity to ACQ 12 that high frequency Lamb waves should be able to localize the surface crack location with a single acquisition node. To test this hypothesis, we will look at results from higher frequency excitation. Figure 50 shows the results for a 155-kHz S_0-mode reconstruction. As hoped, experimental results provide accurate damage detection and localization compared with the actual damage location shown in Figure 51. Figure 52 shows the successful detection of the damage at 145 kHz. Overall, these results show the impressive damage detection and localization capability of the MD7-Pro system combined with advanced processing algorithms.

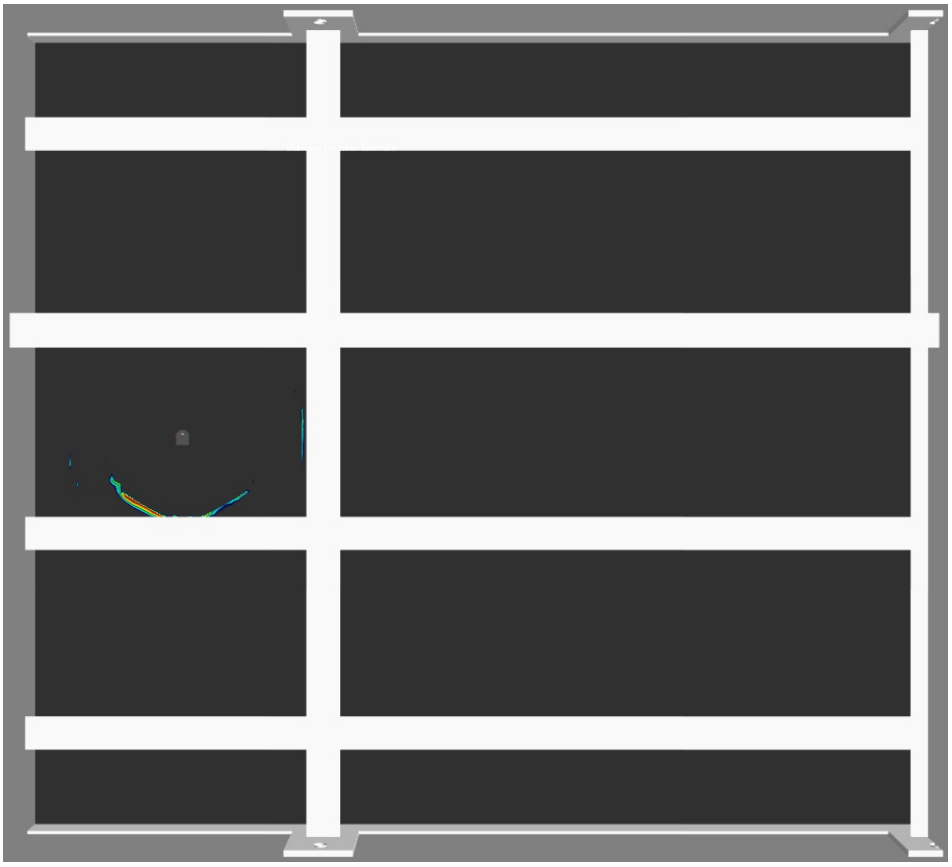

Figure 50. ACQ 12 155-kHz S_0 pulse-echo image map for Damage 6

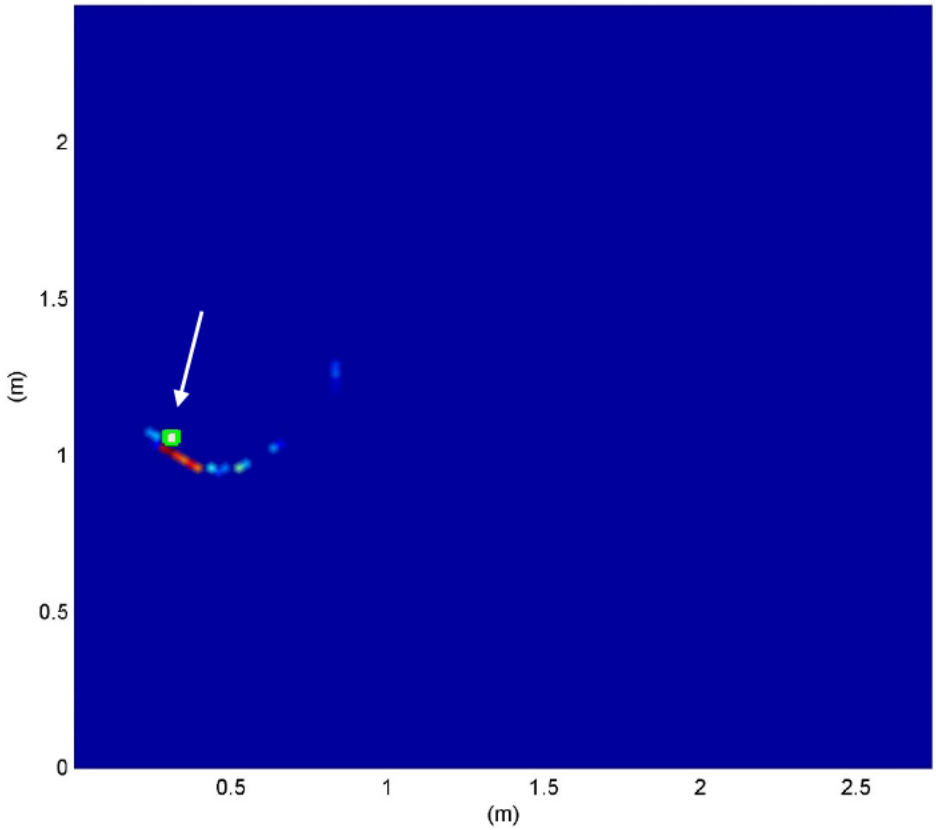

Figure 51. The actual damage location (bright green square) and experimentally determined source of damage shown for 155-kHz S_0 pulse-echo image map of ACQ 12 for Damage 6

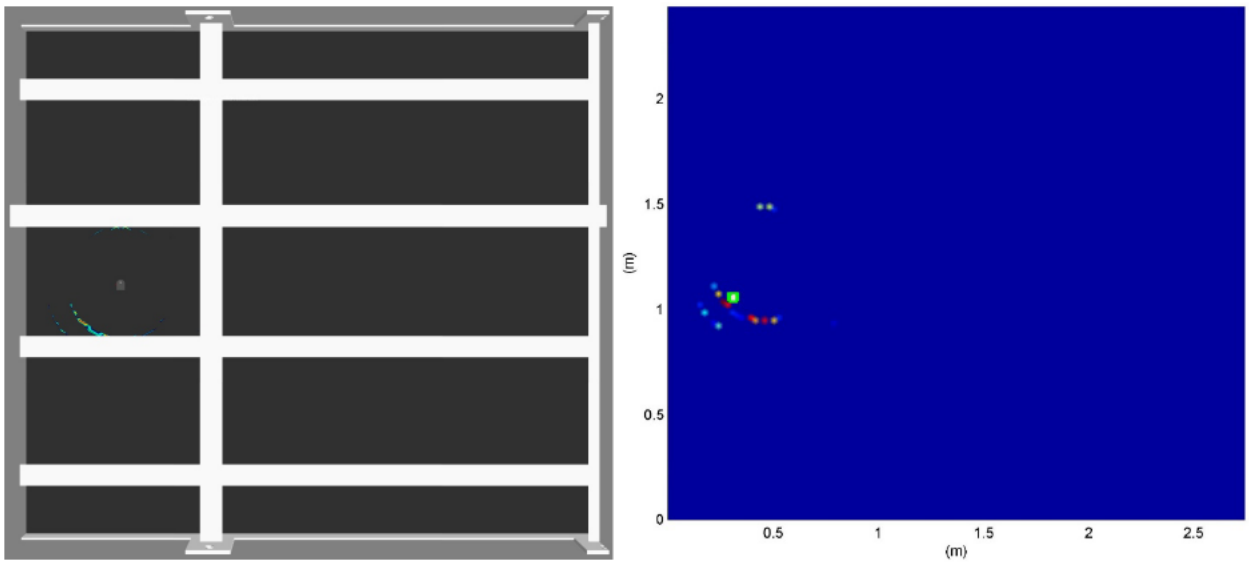

Figure 52. ACQ 12 145-kHz S_0 pulse-echo image map for Damage 6 (left) and actual damage location (right)

6. Conclusions and Recommendations

The value of continuous structural monitoring on ships is becoming more apparent as the information generated from such systems is shared with wider operator and maintenance communities. Ship monitoring is especially valuable for tracking fatigue life and can be of great assistance for extension of ship service life or broader fleet management. However, most of these monitoring systems focus on strain or acceleration responses, which may not provide timely insight into deteriorating structural integrity. For a more complete view of structural condition, regular visual or nondestructive inspections can be used to provide more insight into the material and structural condition. However, such inspections are costly and typically only available when ships are in port. To alleviate the need for some manual inspections, actively monitoring the structure for the presence or growth of damage may be one solution. Active SHM also provides the capability to continuously or intermittently monitor stress concentrations, areas that are difficult to physically inspect, or known damage-prone areas. Once structural data streams (global and local load monitoring, temperature, corrosion, sensitization, etc.) are established, a structural digital twin can combine these data with models and machine learning to provide continuous forecasting of future ship health in timescales ranging from remaining useful life to the probability of current mission success.

6.1 Brief Report Summary

The U.S. Navy and other organizations have been contracting with small businesses to develop SHM sensors, hardware, algorithms, and software for many years. In this study, small-business-developed SHM hardware, recently licensed and produced by a major aerospace component and system supplier, is evaluated for use on surface ships. After purchasing hardware from the new manufacturer, four sensors and nodes were installed on a large, welded steel grillage. An analysis of experimental wave propagation properties revealed which Lamb wave modes at which frequencies may be sensitive to localized stiffness changes (damage) in the structure. After a series of artificial defects were introduced, advanced algorithms incorporating beamforming techniques were used to analyze the collected results. Overall, damage detection

results were successful, except in cases where the damage was both small and spatially distant from the sensing nodes.

6.2 Key Findings

With respect to the research objective to evaluate a COTS SHM solution for use in maritime environments, these findings will be separated into two categories: hardware and software. The guided-wave SHM hardware as produced by Collins Aerospace is an incremental improvement over the previous version, and it is significantly improved over earlier prototypes produced almost exclusively under SBIR and STTR contracts. The Navy and other sponsors provided significant feedback to Metis Design Corporation, resulting in numerous improvements to hardware durability, installation methods, connectors, wiring, and other features. After licensing the hardware, Collins Aerospace modified circuit designs and components to meet their stringent aerospace component standards and utilize their existing production supply chain.

The current MD7-Pro Rev 4 hardware is relatively straightforward to install, assemble, and operate for collecting data. The installation tool greatly eases the structural sonar installation process, and anyone familiar with installing strain gauges or similar surface-bonded sensors should quickly learn the proper technique. The only difficulty with installation occurred when trying to use the incorrect installation tool. The tabs on the structural sonar circuit can be broken if not using the latest tool. Attaching the acquisition nodes and cables is straightforward with the help of markings and alignment tabs on the sensor nodes and matching shapes and slots on the acquisition nodes. The only production issues noted were that the actuator on one of structural sonar nodes had an intermittent connection, and one uninstalled sonar node also had a bad electrical connection to the actuator.

Purchase, installation, setup, and data collection with the MD7-Pro hardware should be straightforward for most engineers and technicians. There are some caveats to this statement. To fully use the capability of the structural sonar nodes, the user will likely need some understanding of, or experience with, experimental wave propagation. The same prerequisites are also likely true if using the hardware for passive acoustic

emission or impact localization monitoring, where the system does not provide an active excitation into the host structure. However, the system can also be used as a fully digital, distributed data acquisition system for strain, temperature, vibration, crack gauges, etc. In that sense, the MD7-Pro Rev 4 hardware is compact and extremely capable to any user familiar with sensor data acquisition.

In this study, the accumulator node and a laptop interfaced with the rest of the hardware. For a shipboard or long-term application, Collins Aerospace is pairing the structural sensing subsystem (accumulator nodes, acquisition nodes, and sensing nodes) with a broader pulse health monitoring system (PHMS), which is a scalable data collection and processing line replaceable unit (LRU). The LRU can be swapped for data transfer, has several internal data transfer protocols, both wired and wireless, and the capability for local data processing. An investigation with the broader system is briefly detailed in the next section.

The second category of findings relates to the data analytic and visualization software. In this study, the executable generated to process the grillage data was generated via collaboration with Metis Design Corporation. For a limited study such as this, this arrangement is not a significant burden. If using the system at scale, the means of data analysis and damage visualization is likely the largest roadblock to overcome. Collins Aerospace has focused on improving the hardware and its operating software. At this time, there does not appear to be a COTS software solution ready to perform the data analysis for any generic structure of interest. Ideally, a user-friendly software tool that can import structural models, map physical sensor node locations, process data, and provide visualization of the results will be developed and made available. In the near term, data processing functionality may need to be an internal engineering service or outsourced as bespoke analysis tools specific to the application. The latter solution becomes logistically challenging when dealing with sensitive ship structures typical of naval or proprietary commercial vessel applications.

6.3 Future Work Recommendations

One of the original goals of this work was to investigate long-term, continuous operation of the COTS SHM system. After proposing the extended testing, discovery of

the inclusion of the structural sensing components into a larger, commercial health and usage monitoring system resulted in postponement of the effort until the full system could be evaluated. There are plans currently under consideration to deploy a shipboard evaluation of the MD7-Pro structural sensing system with a Collins PHMS.

As previously noted, the installed sensor layout enabled maximum spatial coverage of the grillage structure. In retrospect, it may have been more prudent to focus on one or two details of interest, such as longitudinal and transverse stiffener intersections. Sensor nodes with closer spacing in a thick, welded structure would allow the opportunity to view damage progression (crack growth, corrosion) and provide less uncertainty and higher confidence with respect to damage localization. Assessing individual details would also allow for the utilization of higher order Lamb wave modes. The higher order modes have shorter wavelengths, which attenuate more quickly in the structure. However, those shorter wavelengths would also be more sensitive to smaller structural defects. A wider range of test structures, materials, and sensor layouts are slated for future experiments.

Related to investigating specific details of interest, the aerospace community has successfully implemented sensor-based monitoring for prognostic purposes. While much of the monitoring infrastructure is not specifically for structures, integrated sensing hardware has provided improved asset availability, extended service-life, and reduced operating costs of the monitored structures. Part of the success of these programs is the confidence in the hardware and sensors to adequately detect and characterize the onset and progression of failure mechanisms. For ship maintenance and classification communities, similar research is critical for expressing confidence in the findings from damage detection systems. A larger study should be conducted to determine high-priority locations and details (stress concentrations, fatigue prone, etc.), which are suitable for active damage detection monitoring, across ship classes. For the identified details, full material and damage mechanism characterizations can be performed. Finally, a probability of detection (PoD) study, following the formal statistical framework laid out in MIL-HDBK-1823A, should be completed. PoD studies at Naval Air Systems Command and NASA with SHM hardware have led to successful integration of new sensing paradigms with statistically based confidence intervals in the results.

Finally, the capabilities and hardware packaging of the MD7-Pro Rev4 are under revision by Collins Aerospace. It is expected that the MD7-Pro hardware will be replaced with a new evolution of the hardware in the near future. As such, a study similar to the one conducted in this investigation will need to be undertaken with the new system. While the current system already meets many standard military specifications and requirements, the next generation hardware should be further tested to ensure shipboard specific requirements such as shock, smoke and toxicity, and electromagnetic compatibility.

6.4 Future Digital Twin Integration

The output generated from the damage detection and characterization technology described in this report is but one of many inputs included in the concept of a structural digital twin. As Glaessgen and Stargel (2012) envisioned, a digital twin for structures encompasses “integrated multiphysics, multiscale, probabilistic simulation of an as-built vehicle or system that uses the best available physical models, sensor updates, fleet history, etc., to mirror the life of its corresponding [operational] twin.” In other terms, understanding when and where damage may have initiated while a ship is operational is a critical data stream, but it is one of many required measurements to achieve the capability of continually forecasting structural health, time-to-maintenance, probability of mission success, remaining useful life, and other prognostic calculations.

Other critical components of a digital twin include environmental (wave, solar) loads, global and local ship response to those loads, and physics-based numerical models and can range in fidelity from hand-written notes on the corrosion wastage of plating to 3D point cloud data developed from scanning the surface of a plate with deformities. All of these measurements and modeling techniques introduce some level of uncertainty when introducing them to a multiscale, multifidelity simulation, but early results have shown the value of continuous measurements with respect to only relying upon decisions made during the design and conceptualization of a physical asset (Mondoro and Grisso, 2019).

In the larger structural digital twin paradigm, the monitoring of damage initiation and growth is a narrow, but potentially critical, source of information necessary for

maintaining a comprehensive twin. While the hardware detailed in this report is capable of acquiring other data needed for a full understanding of the operational asset (wave-induced strain and ship motions, distributed temperature, etc.), these results and guidelines have a narrowed focus limited only to detecting and characterizing structural damage. With these assumptions and boundaries laid out, the following is a conceptual view of how active damage detection will eventually be incorporated into a broader ship structure digital twin.

6.4.1 Define Damage Monitoring Locations

The first step is to identify structural areas, details, and joints that would benefit from a damage detection schema. For several reasons, ranging from practicality to cost to the sheer amount of data produced, the use of active damage detection techniques is not likely to cover the structure of an entire ship. Near-term usage will, therefore, focus on targeted structural details of interest. Areas of concern could be identified from areas of known stress concentrations or high fatigue accumulation, areas with prior proclivity to damage during operational use (hot spots), or locations which are simply difficult to inspect.

6.4.2 Calibrate Sensing System

Once critical locations for monitoring have been identified, the next step is to thoroughly study each detail. Crucial questions to ask about the structure include the following: How and of what materials is the joint constructed? How is loading applied in operation? What are the primary damage mechanisms and most likely locations of damage initiation? These details are necessary to characterize wave propagation in the material and, thus, the ability to detect specific defects and to assist with development of any necessary custom damage-detection algorithms. As previously mentioned, this is the step where a probability of detection study would be performed to provide a formal statistical framework to evaluate detectability for the relevant damage mechanisms. Sensor placement optimization routines can assist in defining the amount and location of sensor nodes.

6.4.3 System Installation and Operation

Based on the analytical and numerical studies performed in the previous section, the next step in implementing active damage detection is to physically install the sensors in the previously determined optimal locations. The system could be set up to collect data at defined intervals or on demand, including an active scan triggered by a detected acoustic emission event. Along with the actual sensors and hardware, a numerical model of the physical detail should accompany the sensor installation. The model is used to interpret sensing results to provide the statistically based, most likely damage conditions and pass along any changes to the larger digital twin. Ideally, this localized detail model is contained at the edge, either at the sensor location or in a common computing resource on the ship. Any indications of damage, with its corresponding statistical uncertainty, would be fed into the larger afloat digital twin manager. The digital twin manager should have a model-updating engine to autonomously modify the condition of the ship structure for use in engineering analyses. Afloat digital twins could have data from both localized detail condition as well as current global ship response, environmental conditions, and more to inform operators of ship health. The structural information can be combined with information from other ship systems to generate system-of-systems digital twins for enhanced awareness of current and predicted future conditions for use in mission planning assessments. Likely damage locations, ship usage and fatigue accumulation, overload events, etc. are relayed to the corresponding ashore digital twin for mission planning, maintenance planning, fleet management, and ship life cycle decisions.

To achieve this vision of afloat and ashore digital twins of ship structure, several technology enhancements are necessary. Shipboard edge computing will be necessary to process the damage detection data and update the individual joint surrogate or reduced-order models. The models themselves will need an automated updating engine to change the local models before new numerical calculations can be performed. Finally, to reach prognostic capability, data fusion techniques of disparate data streams must exist to understand how the ship structure will perform in the current and future missions, based on ship condition, expected operational environment, and other conditions.

Acknowledgments

I am grateful to the Ship Structure Committee (SSC) for taking interest in structural health monitoring for ships and providing a pathway for this research to develop. I specifically thank Mr. David Qualley (NAVSEA 05P) for chairing the Project Technical Committee (PTC), organizing the meetings, and keeping the project on track. I am grateful to the rest of the PTC for providing valuable feedback and suggestions throughout the duration of this project. NAVSEA 05 Cross Platform Systems Development program provided funding for this project. The test structure used was fabricated and previously tested under an Office of Naval Research (ONR) program sponsored by Dr. Paul Hess (ONR 331).

I would like to acknowledge the following individuals for their invaluable contributions to this effort. Ms. Hannah Donakowski and Mr. Nazir Shamsiev supported the setup of this study during their internship periods. Mr. David Leasure provided valuable assistance enabling the usage of the test structure. Dr. Seth Kessler and Dr. Greg Jarmer of Metis Design Corporation assisted with developing the analysis software. Finally, Mr. Kevin Hawko, Mr. Brian Gebo, Mr. Ben Witham, and Mr. Jie Pan of Collins Aerospace assisted with the hardware purchase and initial hardware troubleshooting.

References

American Bureau of Shipping, 2016. "ABS Rules and Guides Archives: Guide for Hull Condition Monitoring Systems," Available: https://ww2.eagle.org/content/dam/eagle/rules-and-guides/current/conventional_ocean_service/73_Hull_Condition_Monitoring_2016/hull-condition-monitoring-guide-e-mar16.pdf. [Accessed 10 July 2018].

American Bureau of Shipping, 2018. "ABS to pilot bow-to-stern Condition-Based Class for U.S. Navy's MSC," Available: https://ww2.eagle.org/en/news/press-room/abs-to-pilot-bow-to-stern-condition-based-class-for-us-navy-msc.html. [Accessed 10 July 2018].

Achenbach, J. D., 1973. *Wave Propagation in Elastic Solids*, Elsevier Science Publishers B.V., Amsterdam.

Adams, D. E., 2007. *Health Monitoring of Structural Materials and Components: Methods with Applications*, John Wiley & Sons Inc., Hoboken, NJ.

Collins Aerospace, 2016. “UTC Aerospace Systems Acquires License for Structural Health Monitoring System,” Available: http://www.utc.com/News/UTAS/Pages/UTC-Aerospace-Systems-acquires-license-for-structural-health-monitoring-system-te.aspx. [Accessed 10 January 2017].

Collins Aerospace, 2018. “MD7-Pro Digital Structural Health Monitoring System Usage Manual.”

Diligent, O., Grahn, T., Bostrom, A., Cawley, P., and Lowe, M. J. S., 2002. “The low-frequency reflection and scattering of the S0 Lamb mode from a circular through-thickness hole in a plate: finite element, analytical and experimental studies,” *Journal of the Acoustical Society of America*, Vol. 112, No. 6, pp. 2589–2601.

Doherty, J. E., 1987. “Nondestructive Evaluation,” Chapter 12 in: Kobayashi, A. S. (Editor), *Handbook on Experimental Mechanics*, Prentice-Hall, Inc., Englewood Cliffs, NJ.

Drazen, D. A., Mondoro, A. M., and Grisso B. L., 2019. “Use of Digital Twins to Enhance Operational Awareness and Guidance,” 18th Conference on Computer and IT Applications in the Maritime Industries, March 25-27, Tullamore, Ireland, pp. 344-351.

Drummen, I. Grasso, N., and Stambaugh, K., 2016. “Validation of Hydro-Structural Coupling with Full Scale Data,” The Society of Naval Architects and Marine Engineers Maritime Convention, Nov. 1-5, Bellevue, WA.

Farrar, C. R., and Worden, K. 2007. “An introduction to structural health monitoring,” *Philosophical Transactions of the Royal Society A,* Vol. 365, pp. 303–315.

Flynn E. B., Todd M. D., Dunn C. T., and Kessler, S. S., 2011. "Identifying Scatter Targets in 2D Space using In Situ Phased-Arrays for Guided Wave Structural Health Monitoring." Proceedings of the 8th International Workshop on Structural Health Monitoring, September 12-15, Stanford University.

Fromme, P. and Sayir, M. B., 2002. Measurement of the scattering of a Lamb wave by a through hole in a plate, *Journal of the Acoustical Society of America*, Vol. 111, No. 3, pp. 1165–1170.

Giurgiutiu, V., 2014. *Structural Health Monitoring with Piezoelectric Wafer Active Sensors*, Academic Press, New York.

Glaessgen, E. and Stargel, D., 2012. “The digital twin paradigm for future NASA and US Air Force vehicles,” 53rd AIAA/ASME/ASCE/AHS/ASC Structures, Structural Dynamics and Materials Conference 20th AIAA/ASME/AHS Adaptive Structures Conference 14th AIAA. pp. 1818.

Grisso, B. L., Salvino, L. W., Singh, G., Singh, G, Tansel, I. N., 2011a. “A comparison of impedance and Lamb wave SHM techniques for monitoring structural integrity of and through welded joints,” Proceedings of SPIE Volume 7984.

Grisso, B. L., Park, G., Salvino, L. W., and Farrar, C. R., 2011b. "Structural Damage Identification in Stiffened Plate Fatigue Specimens Using Piezoelectric Active Sensing," Proceedings of the 8th International Workshop on Structural Health Monitoring, September 13-15, Stanford, CA, pp. 1683-1690.

Grisso, B. L., 2013. “Development of a Structural Health Monitoring Prototype for Ship Structures,” Ship Structure Committee, SSC-468.

Hess, P. E., 2007. “Structural Health Monitoring for High-Speed Naval Ships,” Proceedings of the 6th International Workshop on Structural Health Monitoring, Sept. 11-13, Stanford, CA, pp. 3-15.

Inman, D. J., Farrar, C. R., Lopes, Jr., V., and Steffen, Jr., V., 2005. *Damage Prognosis: For Aerospace, Civil and Mechanical Systems,* John Wiley & Sons, Ltd., Chichester, UK.

Jarmer, G. J. S., Flynn E. B., and Todd, M. D., 2014. “Multi-wave-mode, Multi-Frequency Detectors for Guided Wave Interrogation of Plate Structures,” *Structural Health Monitoring*, Vol. 13, No. 2, pp. 120-130.

Kessler S. S., Flynn E. B. and M. D. Todd, 2011a. "Hybrid Coherent/Incoherent Beam Forming Diagnostic Approach to Naval Assets." Proceedings of the 8th International Workshop on Structural Health Monitoring, September 12-15, Stanford University.

Kessler S. S., Flynn E. B., Dunn C. T., and Todd, M. D., 2011b. "A Structural Health Monitoring Software Tool for Optimization, Diagnostics and Prognostics." Proceedings

of the 3nd Annual Conference of the Prognostics and Health Management Society, September 25-29, Montreal, Quebec.

Lamb, H., 1917. “On Waves in an Elastic Plate,” *Proceedings of the Royal Society of London*, Vol. 93, No. 648, pp. 114-128.

MarEx, 2018. "The Maritime Executive: ABS and MSC Trial Condition-Based Class," Available: https://www.maritime-executive.com/article/abs-and-msc-trial-condition-based-class. [Accessed 10 July 2018].

McKeon, J. C. P. and Hinders, M. K., 1999. “Lamb Wave Scattering From a Through Hole,” *Journal of Sound and Vibration*, Vol. 224, No. 5, pp. 843-862.

Metis Design Corporation, 2013. “Guided Wave-based SHM of Submersible Navy Composites,” Contract N00024-13-C-4050. Available: https://www.sbir.gov/sbirsearch/detail/415715. [Accessed 5 December 2019].

Metis Design Corporation, 2019. “MD7 PRO Digital SHM System,” Available: https://www.metisdesign.com/structural-health-monitoring-company/md7-digital.html. [Accessed 5 December 2019].

Military Detail Specification [MIL-DTL]-32139B, 2017. Department of Defense Detail Specification: GENERAL SPECIFICATION FOR CONNECTORS, ELECTRICAL, RECTANGULAR, NANOMINIATURE, POLARIZED SHELL. Available: https://landandmaritimeapps.dla.mil/Downloads/MilSpec/Docs/MIL-DTL-32139/dtl32139.pdf. [Accessed 5 December 2019].

Military Standard [MIL-STD]-790, 2018. Department of Defense Standard Practice: ESTABLISHED RELIABILITY AND HIGH RELIABLITY QUALIFIED PRODUCTS LIST (QPL) SYSTEMS FOR ELECTRICAL, ELECTRONIC, AND FIBER OPTIC PARTS SPECIFICATIONS. Available:

https://landandmaritimeapps.dla.mil/Downloads/MilSpec/Docs/MIL-STD-790/std790.pdf. [Accessed 5 December 2019].

Mondoro, A. M. and Grisso, B. L., 2019. “On the integration of SHM and digital twin for the fatigue assessment of naval surface ships,” Proceedings of the 12th International Workshop on Structural Health Monitoring, September 10-12, Stanford, CA.
Moreau, L. Caleap, M., Velichko, A., and Wilcox, P. D., 2011. “Scattering of guided waves by through-thickness cavities with irregular shapes,” *Wave Motion*, Vol. 48, pp. 586-602.

Small Business Innovation Research Topic N111-053 [2011], “Structural Health Monitoring of Submersible Navy Composites,” Available: https://www.navysbir.com/n11_1/N111-053.htm. [Accessed 5 Dec 2019].

Rose, J. L., 2014. *Ultrasonic Guided Waves in Solid Media*, Cambridge University Press, New York.

Salvino, L. W. and Brady, T. F., 2007. “Hull Structure Monitoring for High-Speed Naval Ships,” Proceedings of the 6th International Workshop on Structural Health Monitoring, Sept. 11-13, Stanford, CA, pp. 1465-1472.

Schiere, M., Bosman, T., Derbanne, Q., Stambaugh, K., and Drummen, I., 2017. Sectional load effects derived from strain measurements using the modal approach, *Marine Structures,* Vol. 54, pp. 188-209.

Swartz, R. A., Zimmerman, A. T., Lynch, J. P., Rosario, J., Brady, T. F., Salvino, L. W., and Law, K. H., 2010. “Hybrid wireless hull monitoring system for naval combat vessels,” *Structure and Infrastructure Engineering: Maintenance, Management, Life-Cycle Design and Performance*, Vol. 6, No. 3, pp. 1-18.

Waveform Revealer 3, University of South Carolina Laboratory For Active Materials and Smart Structures, Available: http://www.me.sc.edu/research/lamss/html/software.html. [Accessed 5 Dec 2019].

Appendix A

Annotated Grillage Run File in “Tables” Directory

START = off	
BUS = R	Turn on power to the right bus
RUN = PE_11.gwmode	Run the pulse-echo guided-wave profile on ACQ 11
PAUSE = 10	Pause 10 s
RUN = PE_12.gwmode	Run the pulse-echo guided-wave profile on ACQ 12
PAUSE = 10	Pause 10 s
RUN = PC_11_12.gwmode	Run the pitch-catch guided-wave profile from ACQ 11 to ACQ 12
PAUSE = 10	Pause 10 s
RUN = PC_12_11.gwmode	Run the pitch-catch guided-wave profile from ACQ 12 to ACQ 11
PAUSE = 10	Pause 10 s
BUS = L	Turn on power to the left bus
RUN = PE_13.gwmode	Run the pulse-echo guided-wave profile on ACQ 13
PAUSE = 10	Pause 10 s
RUN = PE_14.gwmode	Run the pulse-echo guided-wave profile on ACQ 14
PAUSE = 10	Pause 10 s
RUN = PC_13_14.gwmode	Run the pitch-catch guided-wave profile from ACQ 13 to ACQ 14
PAUSE = 10	Pause 10 s
RUN = PC_14_13.gwmode	Run the pitch-catch guided-wave profile from ACQ 14 to ACQ 13
BUS = off	Turn off bus power
STOP = on	End test

Example Pitch-Catch Guided-Wave Mode in the “Modes” Directory (“PC_11_12.gwmode”)

11=pitch.gw	Defines ACQ 11 as the actuation node
12=catch.gw	Defines ACQ 12 as the sensing node

Example Pulse-Echo Guided-Wave Mode in the “Modes” Directory (“PE_11.gwmode”)

11=pulse.gw	Defines ACQ 11 as the actuation node
11=echo.gw	Defines ACQ 11 as the sensing node

Pitch Guided-Wave Parameters in the “Profiles” Directory (“pitch.gw”)

act_type=2	Defines the actuation type to Chirp
act_vpp=20	Defines the peak-to-peak actuation voltage to 20
sample_time_us=1000	Sets the sampling time to 1000 μs
gain=3	Sets the signal gain to 3
avg_power=9	Sets the number of averages to 2^9 (512 averages)

Catch Guided-Wave Parameters in the “Profiles” Directory (“catch.gw”)

act_type=0	Defines the node as a sensor
sample_time_us=1000	Sets the sampling time to 1000 µs
gain=150	Sets the signal gain to 3
avg_power=9	Sets the number of averages to 2^9 (512 averages)

Pulse Guided-Wave Parameters in the “Profiles” Directory (“pulse.gw”)

act_type=2	Defines the actuation type to Chirp
act_vpp=20	Defines the peak-to-peak actuation voltage to 20
sample_time_us=1000	Sets the sampling time to 1000 µs
gain=3	Sets the signal gain to 3
avg_power=9	Sets the number of averages to 2^9 (512 averages)

Echo Guided-Wave Parameters in the “Profiles” Directory (“echo.gw”)

act_type=0	Defines the node as a sensor
act_vpp=20	Defines the peak-to-peak actuation voltage to 20
sample_time_us=1000	Sets the sampling time to 1000 µs
gain=4	Sets the signal gain to 4
avg_power=9	Sets the number of averages to 2^9 (512 averages)

Appendix B

Figure 53 through Figure 57 show photographs of the damage cases not contained within the main report body.

Figure 53. Damage 2, a simulated transverse stiffener weld toe crack (top) and its relation to ACQ 13 (bottom)

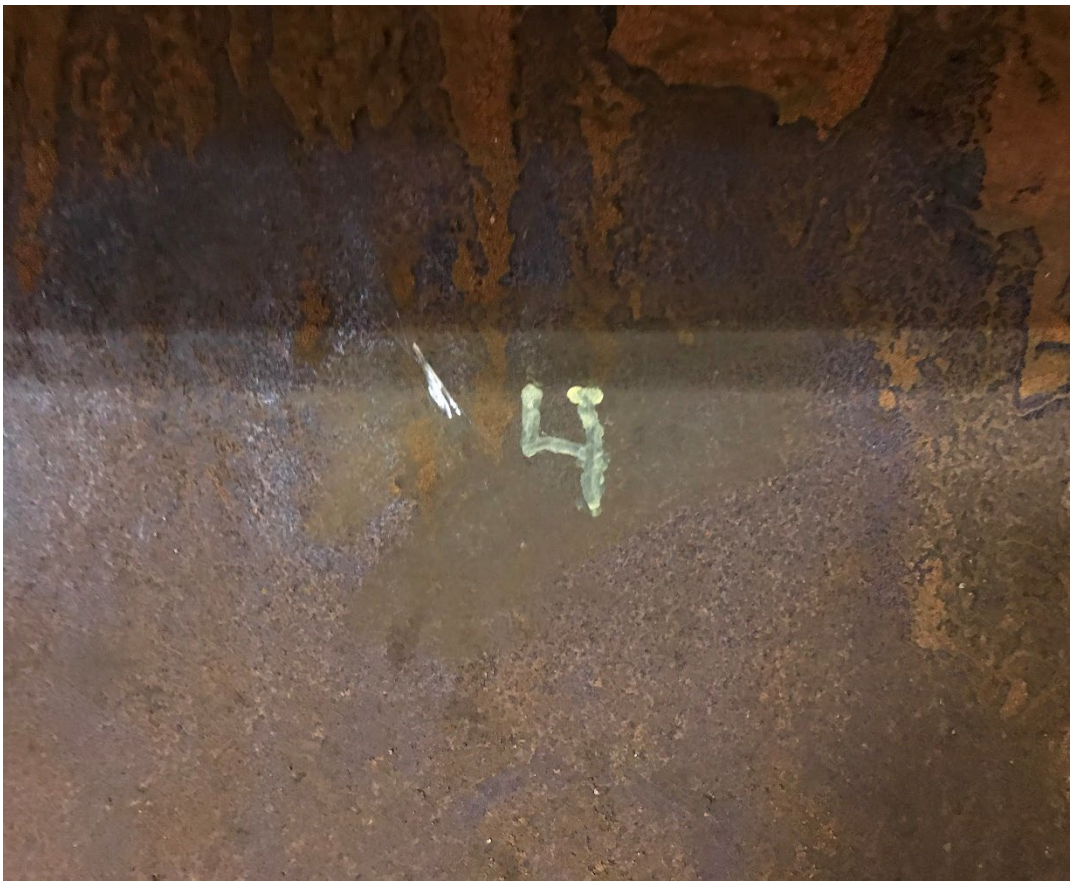

Figure 54. Damage 4, a simulated baseplate surface crack

Figure 55. Damage 5, a simulated transverse stiffener weld toe crack

Figure 56. Damage 4 and Damage 5 in relation to ACQ 14

Figure 57. Damage 6, a simulated plate crack, in relation to ACQ 12